Research Square

Preprints are preliminary reports that have not undergone peer review.
They should not be considered conclusive, used to inform clinical practice,
or referenced by the media as validated information.

A Radius-Decoder-assisted Constrained Multi-Objective Evolutionary Algorithm for Probabilistic Strong Barrier Coverage in Multimedia Wireless Sensor Networks

Nguyen Thi My Binh
Hanoi University of Industry
Nguyen Quang Huy
Hanoi University of Science and Technology
Nguyen Thi Hue
Hanoi University of Science and Technology
Dao Khac Hoang Vu
National University of Singapore
Ho Viet Duc Luong
luonghvd@soict.hust.edu.vn

Hanoi University of Science and Technology

Research Article

Keywords: Probabilistic barrier coverage, sep wireless sensor networks, sep multi-objective optimization, sep evolutionary algorithms

Posted Date: October 9th, 2026

DOI: https://doi.org/10.21203/rs.3.rs-10181688/v1

License: This work is licensed under a Creative Commons Attribution 4.0 International License.
Read Full License

Additional Declarations: No competing interests reported.

A Radius-Decoder-assisted Constrained Multi-Objective Evolutionary Algorithm for Probabilistic Strong Barrier Coverage in Multimedia Wireless Sensor Networks

Nguyen Thi My Binh[1], Nguyen Quang Huy[2], Nguyen Thi Hue[2], Dao Khac Hoang Vu[3], Ho Viet Duc Luong[2*]

[1]Hanoi University of Industry, Hanoi, 100000, Vietnam.
[2]Hanoi University of Science and Technology, Hanoi, 100000, Vietnam.
[3]National University Singapore, 119077, Singapore.

*Corresponding author(s). E-mail(s): luonghvd@soict.hust.edu.vn;
Contributing authors: binhntm@haui.edu.vn;
huy.nq230039@sis.hust.edu.vn; hue.nt237439@sis.hust.edu.vn;
daokhachoangvu@u.nus.edu;

Abstract

Strong barrier coverage is a fundamental requirement in wireless sensor networks for intrusion detection and perimeter surveillance. In practical deployments, deterministic disk sensing models are often too idealized because sensing quality gradually decreases with distance and multiple sensors may jointly contribute to the detection of a barrier point. This paper studies the bi-objective probabilistic strong barrier coverage problem, where the number of active sensors and the total energy consumption are minimized simultaneously while satisfying a continuous sensing-intensity constraint along the protected barrier. To address the mixed binary–continuous and highly constrained nature of this problem, we propose RDC-MOEA, a radius-decoder-assisted constrained multi-objective evolutionary framework. Instead of directly optimizing both sensor activation and sensing radii, RDC-MOEA evolves binary activation patterns and uses a problem-specific RadiusFormalize decoder to construct the corresponding uncertainty-radius configurations. This design reduces the effective search space and incorporates coverage-feasibility handling into the decoding process. We instantiate the framework with an NSGA-II backbone and compare it with decoder-assisted MOEA/D and NSPSO variants under the same

representation and evaluation protocol. Experimental results on randomly generated barrier instances show that the NSGA-II-based RDC-MOEA achieves the best overall performance, obtaining higher Hypervolume, lower IGD, and better Spread Delta values than the compared variants. The ablation study further confirms that replacing RadiusFormalize with a common-radius decoder leads to clear performance degradation, demonstrating the importance of adaptive radius formalization. Sensitivity analysis under different detection thresholds, attenuation coefficients, and sensing-radius ratios also shows that the proposed method remains robust across a range of probabilistic sensing conditions. These results demonstrate the effectiveness of combining problem-specific radius decoding with dominance-based multi-objective evolutionary search for approximating active-count–energy trade-offs in probabilistic strong barrier coverage.

Keywords: Probabilistic barrier coverage wireless sensor networks multi-objective optimization evolutionary algorithms

1 Introduction

Wireless sensor networks (WSNs) have been widely adopted in surveillance, environmental monitoring, industrial inspection, and security-sensitive applications, where distributed sensors are deployed to continuously monitor large physical regions [1–3]. In such systems, coverage, connectivity, and energy efficiency are fundamental requirements that directly determine whether the deployed network can reliably monitor the region or boundary of interest over time [4–8]. Among different coverage models, barrier coverage is particularly important for intrusion detection and perimeter protection. Unlike area coverage, which aims to monitor every point in a two-dimensional region, barrier coverage focuses on forming a sensing barrier that intersects any crossing path of an intruder [1, 9]. A stronger form, known as strong barrier coverage [10, 11], requires that every possible crossing of the protected barrier can be detected with a prescribed level of sensing reliability.

Most existing studies on barrier coverage adopt deterministic disk sensing models, where a sensor is assumed to fully cover all points within a fixed sensing radius and to provide no coverage outside that radius [12, 13]. Although this abstraction simplifies analysis and algorithm design, it is often too idealized for practical sensing environments. In real deployments, sensing quality usually degrades gradually with distance because of signal attenuation, measurement noise, and environmental uncertainty [14]. Probabilistic sensing models address this limitation by assigning each sensor a distance-dependent sensing contribution [14]. Under this model, a barrier point may be jointly monitored by multiple sensors, and its coverage status should be determined by the aggregate sensing intensity rather than by a single binary coverage decision. As a result, probabilistic strong barrier coverage imposes a continuous feasibility requirement: every point along the barrier must receive sufficient aggregate sensing intensity. Maintaining such a strong probabilistic barrier is inherently resource-constrained. Activating more sensors can improve sensing robustness and reduce local coverage gaps, but it also increases operational cost and may shorten network lifetime

[7, 15–17]. Conversely, activating fewer sensors reduces the number of operating nodes, but the selected sensors may need larger sensing radii to compensate for uncovered intervals, leading to higher energy consumption [4, 18]. Therefore, sensor activation and radius assignment naturally form a bi-objective optimization problem, where the number of active sensors and the total energy consumption should be minimized simultaneously while preserving probabilistic strong barrier coverage. This trade-off is nontrivial because the problem combines binary activation decisions, continuous radius-dependent energy costs, and a coverage constraint defined over infinitely many points along the barrier.

Multi-objective evolutionary algorithms (MOEAs) are suitable candidates for such problems because they can approximate a set of Pareto-optimal trade-off solutions instead of returning a single scalarized solution [19, 20]. This property is attractive for WSN coverage optimization, where different deployment preferences may favor different compromises between sensor sparsity and energy efficiency. However, applying a generic MOEA directly to the problem remains challenging. If both activation variables and sensing radii are optimized simultaneously, the search space becomes mixed discrete–continuous and highly constrained. Moreover, standard variation operators may frequently generate infeasible configurations that leave some portions of the barrier insufficiently covered. These observations indicate that an effective algorithm should exploit the structure of the barrier coverage problem rather than treating sensor activation and radius assignment as independent decision components. To address these challenges, we propose **RDC-MOEA**, a *Radius-Decoder-assisted Constrained Multi-Objective Evolutionary Algorithm* for probabilistic strong barrier coverage in WSNs. The main idea is to decouple the combinatorial activation search from the continuous radius assignment process. Instead of evolving both the binary activation vector and the sensing radii, RDC-MOEA evolves only the binary activation vector. For each activation, a problem-specific radius decoder constructs a corresponding radius configuration that aims to satisfy the probabilistic strong barrier coverage constraint with low energy consumption. In this way, the evolutionary search focuses on meaningful activation structures, while feasibility handling and energy-aware radius assignment are performed through a deterministic problem-informed decoding procedure.

The main contributions of this paper are summarized as follows:

- We formulate the *Bi-objective Probabilistic Strong Barrier Coverage* problem, abbreviated as **B-PSBC**, in which the number of active sensors and the total energy consumption are minimized subject to a continuous probabilistic strong barrier coverage constraint.
- We propose **RDC-MOEA**, a radius-decoder-assisted constrained multi-objective evolutionary framework that decouples binary sensor activation from sensing-radius assignment.
- We design a problem-specific radius decoder that maps each activation vector to a feasible radius configuration, thereby providing a feasibility-oriented evaluation mechanism for probabilistic strong barrier coverage.

- We instantiate RDC-MOEA with an NSGA-II-based selection mechanism and problem-specific evolutionary operators designed to preserve useful local activation patterns along the barrier.
- We conduct comparative and ablation experiments to evaluate the effectiveness of the proposed radius-decoder-assisted framework against representative multi-objective optimization baselines.

The remainder of this paper is organized as follows. Section 2 reviews related studies on barrier coverage, probabilistic sensing, and multi-objective optimization in WSNs. Section 3 introduces the sensing, intensity, energy, and strong barrier coverage models. Section 4 formally defines the B-PSBC problem. Section 5 presents the proposed RDC-MOEA framework and its radius decoder. Section 6 reports and discusses the experimental results. Finally, Section 7 concludes the paper and outlines possible future research directions.

2 Related Works

Barrier coverage is one of the central coverage models in wireless sensor networks for intrusion detection and perimeter surveillance. It was formally introduced by Kumar et al. [21], who defined a *strong barrier* as a connected belt of sensor coverage that guarantees the detection of any intruder crossing a monitored region. Under the classical deterministic disk sensing model, early studies mainly focused on three directions: verifying the existence of barrier coverage through graph-theoretic methods [9, 22, 23], reducing the number of active sensors through sleep-scheduling mechanisms [8, 24, 25], and repositioning mobile sensors to repair coverage gaps [23, 26, 27]. These studies established important theoretical and algorithmic foundations for barrier coverage. However, their common assumption is that each sensor either fully detects a target inside a fixed sensing radius or completely misses it outside that radius. Such a binary sensing abstraction is convenient for analysis but does not sufficiently capture signal attenuation, environmental interference, and uncertainty in practical sensing environments [3, 28].

Strong barrier coverage has also been extended to heterogeneous and application-specific WSN settings. For example, Binh et al. [9] proposed an exact polynomial-time method for achieving k-strong barrier coverage in heterogeneous wireless multimedia sensor networks. Subsequent studies considered related barrier-coverage problems in rotatable camera sensor networks [11] and three-dimensional underwater WSNs [17], where the objective is often to improve secure lifetime or network lifespan under coverage constraints. Other closely related coverage and connectivity problems have been addressed using genetic algorithms for the maximal exposure path [29], enhanced genetic algorithms for joint lifetime and target coverage in dynamic underwater WSNs [8], mobile device–target association for connectivity enhancement [28], Steiner-tree-based connectivity methods [13], and optimal deployment strategies for hybrid point-and-barrier coverage in heterogeneous sensor networks [30]. Probabilistic sensing models further provide a more realistic alternative by treating detection quality as a distance-dependent quantity. In such models, a barrier point may receive sensing

contributions from multiple nearby sensors, and its coverage status is determined by their aggregate sensing intensity. The work most closely related to ours is that of My and Thi [31], who studied strong barrier coverage in IoT heterogeneous WSNs under a probabilistic sensing model and provided the baseline sensing parameters adopted in this study. However, their formulation combines the conflicting goals of reducing the number of sensors and reducing energy consumption into a single weighted-sum objective. This scalarization strategy has an important limitation: weighted sums may fail to recover Pareto-optimal solutions located in non-convex regions of the Pareto front [32]. Since the trade-off between active sensor count and energy consumption in barrier coverage is generally nonlinear and potentially nonconvex [6, 7], a genuine multi-objective formulation is needed to preserve the full set of trade-off solutions.

Evolutionary algorithms (EAs) have been widely used for WSN coverage and deployment problems because they can approximate a set of non-dominated solutions in a single run [33]. Recent studies have applied hybrid GA–PSO algorithms to obstacle-aware node deployment [3], chaotic gray wolf optimization to coverage and connectivity maximization [6], and deep-learning-assisted optimization methods to coverage enhancement [10, 14]. Among MOEA paradigms, dominance-based methods such as NSGA-II maintain diversity through non-dominated sorting and crowding-distance selection [34], and have been applied to multi-objective routing and WSN coverage–lifetime optimization [3, 10, 35]. Decomposition-based methods such as MOEA/D decompose a multi-objective problem into a set of scalar subproblems and have been widely discussed in constrained MOEA research [36]. Swarm-based approaches, including MOPSO variants, have also been developed to balance convergence and diversity in multi-objective search [37], with applications to energy–coverage trade-offs in heterogeneous WSNs [10, 28]. Nevertheless, the use of MOEAs for probabilistic strong barrier coverage remains limited, especially when the objective is to preserve the full trade-off between the number of active sensors and total energy consumption rather than optimizing a single scalarized objective.

From an algorithmic perspective, probabilistic strong barrier coverage also raises a nontrivial constraint-handling issue. While constraint handling in evolutionary multi-objective optimization has been extensively studied through penalty-based, feasibility-based, and relaxation-based strategies [36], these generic mechanisms may not fully exploit the structural properties of WSN coverage problems. A complementary direction is to embed problem-specific knowledge into the representation or repair procedure. For example, Konstantinidis and Yang [38] designed a constrained evolutionary algorithm based on decomposition for K-connected deployment, illustrating the benefit of incorporating domain structure into the search process. Following this principle, the proposed RadiusFormalize decoder provides a problem-specific feasibility-handling mechanism for probabilistic strong barrier coverage: it restricts the evolutionary search to binary activation patterns and then deterministically constructs the corresponding sensing-radius configuration. This decoder-assisted design reduces the burden on generic constraint-handling operators and enables the same representation to be coupled with different MOEA backbones, including dominance-based, decomposition-based, and swarm-based methods. Overall, prior studies on strong barrier coverage have mainly relied on deterministic disk sensing models, optimized a

single objective, or transformed multiple conflicting objectives into a weighted-sum formulation. In contrast, probabilistic strong barrier coverage with an explicit bi-objective active-count–energy formulation and decoder-based feasibility handling has not been systematically investigated, which motivates the proposed RDC-MOEA framework.

3 Preliminaries

This section introduces the sensing, energy, and barrier-coverage models used throughout the paper. The notation is defined with respect to a one-dimensional barrier, which serves as the basic abstraction adopted in this study for modeling strong barrier coverage in wireless sensor networks.

3.1 Network and Barrier Model

Let $\mathcal{S} = \{s_1, s_2, \ldots, s_N\}$ denote a set of N static sensor nodes deployed to monitor a protected region. The barrier to be protected is represented by a line segment $\mathcal{B} = [0, L]$, where $L > 0$ is the length of the barrier. A point on the barrier is denoted by $x \in \mathcal{B}$. Each sensor s_i is located at position $p_i = (x_i, y_i)$ in the plane. The Euclidean distance from sensor s_i to a barrier point x is defined as

$$d_i(x) = \sqrt{(x_i - x)^2 + y_i^2}. \tag{1}$$

In the special case where all sensors are deployed directly on the barrier line, we have $y_i = 0$ and thus $d_i(x) = |x_i - x|$.

Each sensor can be either active or inactive. Let $u_i \in \{0, 1\}$ be the activation variable of sensor s_i, where $u_i = 1$ indicates that s_i is active and $u_i = 0$ indicates that it is inactive. The activation configuration of the whole network is denoted by

$$\mathbf{u} = (u_1, u_2, \ldots, u_N) \in \{0, 1\}^N. \tag{2}$$

3.2 Probabilistic Sensing Model

In practical wireless sensor networks, sensing quality does not usually change abruptly from full detection to no detection. Instead, detection capability gradually degrades with distance due to signal attenuation, noise, and environmental uncertainty. To capture this effect, we adopt a truncated attenuated-disk sensing model. For each sensor s_i, let $R_{U,i} > 0$ denote its uncertainty detection radius. The corresponding maximum sensing radius is defined as

$$R_{S,i} = kR_{U,i}, \tag{3}$$

where $k > 1$ is a constant controlling the ratio between the maximum sensing radius and the uncertainty detection radius. The certain sensing radius of sensor s_i is therefore

$$R_{S,i} - R_{U,i} = (k - 1)R_{U,i}. \tag{4}$$

The sensing contribution of sensor s_i to a barrier point x is defined as

$$C_i(x; R_{U,i}) = \begin{cases} 1, & \text{if } d_i(x) \le (k-1)R_{U,i}, \\ e^{-\beta\left(d_i(x)-(k-1)R_{U,i}\right)}, & \text{if } (k-1)R_{U,i} < d_i(x) \le kR_{U,i}, \\ 0, & \text{if } d_i(x) > kR_{U,i}. \end{cases} \tag{5}$$

where $\beta > 0$ is the attenuation coefficient. According to this model, a barrier point receives full sensing contribution from s_i if it lies within the certain sensing region. In the uncertainty region, the sensing contribution decreases exponentially with distance. Points outside the maximum sensing radius receive no contribution from s_i. This model generalizes the deterministic disk model by allowing gradual degradation of sensing quality near the boundary of the sensing range.

3.3 Aggregate Sensing Intensity

Since a barrier point may be monitored by multiple active sensors, its coverage status should be evaluated using the aggregate contribution of all active sensors rather than a single-sensor contribution. Given an activation configuration $\mathbf{u}$ and an uncertainty-radius vector

$$\mathbf{r} = (R_{U,1}, R_{U,2}, \ldots, R_{U,N}), \tag{6}$$

the aggregate sensing intensity at point $x \in \mathcal{B}$ is defined as

$$I(x; \mathbf{u}, \mathbf{r}) = \sum_{i=1}^{N} u_i C_i(x; R_{U,i}). \tag{7}$$

A barrier point x is said to be sufficiently covered if its aggregate sensing intensity is not smaller than a prescribed detection threshold $\gamma > 0$, namely

$$I(x; \mathbf{u}, \mathbf{r}) \ge \gamma. \tag{8}$$

The threshold γ controls the required level of sensing reliability. A larger value of γ imposes a stricter coverage requirement and may require more active sensors, larger sensing radii, or both.

3.4 Energy Consumption Model

Energy consumption is a key factor in wireless sensor networks because it directly affects the operational lifetime of the system. In this work, the energy consumed by an active sensor is assumed to depend on its uncertainty detection radius $R_{U,i}$. This model follows the intuition that sensing cost increases with the covered radial extent, while the contribution in the uncertainty region is attenuated with distance. For a sensor with uncertainty detection radius R_U, the energy consumption is modeled as

the sum of two terms:

$$E(R_U) = \int_0^{(k-1)R_U} R\,dR + \int_{(k-1)R_U}^{kR_U} R\exp\left[-\beta\left(R-(k-1)R_U\right)\right]dR. \tag{9}$$

The first integral corresponds to the certain sensing region, where sensing quality is fully maintained. The second integral corresponds to the uncertainty region, where the sensing effect is attenuated exponentially. By evaluating the above expression, the closed-form energy function is given by

$$E(R_U) = \frac{1}{2}\left((k-1)R_U\right)^2 + \frac{(k-1)R_U(1-\omega)}{\beta} + \frac{1-\omega(1+\beta R_U)}{\beta^2}, \tag{10}$$

where $\omega = \exp(-\beta R_U)$. For a network configuration $(\mathbf{u}, \mathbf{r})$, the total energy consumption is defined as

$$E_{\text{net}}(\mathbf{u}, \mathbf{r}) = \sum_{i=1}^{N} u_i E(R_{U,i}). \tag{11}$$

Inactive sensors do not contribute to the total energy consumption.

3.5 Probabilistic Strong Barrier Coverage

Strong barrier coverage requires the protected barrier to be continuously covered so that any intruder crossing the barrier can be detected. Under the probabilistic sensing model, this requirement is expressed through the aggregate sensing intensity over the entire barrier. Given an activation vector $\mathbf{u}$ and a radius vector $\mathbf{r}$, the barrier $\mathcal{B}$ is said to satisfy probabilistic strong barrier coverage if

$$I(x; \mathbf{u}, \mathbf{r}) \geq \gamma, \qquad \forall x \in \mathcal{B}. \tag{12}$$

Equivalently, a configuration is feasible if the minimum sensing intensity over the barrier is at least γ:

$$\min_{x\in\mathcal{B}} I(x; \mathbf{u}, \mathbf{r}) \geq \gamma. \tag{13}$$

This continuous feasibility condition is the central constraint of the probabilistic strong barrier coverage problem. The objective of the optimization process is to find sensor activation and radius configurations that satisfy this condition while reducing the number of active sensors and the total energy consumption.

4 Bi-objective Probabilistic Strong Barrier Coverage Problem

Based on the sensing, intensity, and energy models introduced in Section 3, we formulate the sensor activation and radius assignment task as a bi-objective constrained

optimization problem. The resulting problem is referred to as the *Bi-objective Probabilistic Strong Barrier Coverage* problem, abbreviated as **B-PSBC**. Given a protected barrier $\mathcal{B} = [0, L]$ and a set of static sensors $\mathcal{S} = \{s_1, s_2, \ldots, s_N\}$ deployed around the barrier, the goal of B-PSBC is to determine an activation vector $\mathbf{u}$ and an uncertainty-radius vector $\mathbf{r}$ such that the entire barrier satisfies the probabilistic strong barrier coverage requirement. At the same time, the number of active sensors and the total energy consumption should be minimized.

The first objective is to minimize the number of active sensors:

$$f_1(\mathbf{u}) = \sum_{i=1}^{N} u_i. \tag{14}$$

The second objective is to minimize the total energy consumption of the active sensors:

$$f_2(\mathbf{u}, \mathbf{r}) = \sum_{i=1}^{N} u_i E(R_{U,i}), \tag{15}$$

where $E(R_{U,i})$ is defined in Section 3. For inactive sensors, the assigned uncertainty detection radius is set to zero through the bound

$$0 \le R_{U,i} \le R_U^{\max} u_i, \qquad i = 1, 2, \ldots, N. \tag{16}$$

The B-PSBC problem can be mathematically formulated as follows:
Input:

- N: the number of deployed sensors.
- $P = \{p_1, p_2, \ldots, p_N\}$: the sensor positions, where $p_i = (x_i, y_i)$.
- L: the length of the barrier segment to be protected.
- γ: the sensing-intensity threshold.
- β: the attenuation coefficient.
- k: the sensing-radius ratio, where $R_S = kR_U$.
- $R_U^{\max}$: the maximum uncertainty detection radius.

Output: a set of non-dominated feasible configurations $(\mathbf{u}, \mathbf{r})$ representing different trade-offs between the number of active sensors and the total energy consumption.

$$\min_{\mathbf{u},\,\mathbf{r}} \quad \mathbf{F}(\mathbf{u}, \mathbf{r}) = \big(f_1(\mathbf{u}), f_2(\mathbf{u}, \mathbf{r})\big) \tag{17a}$$

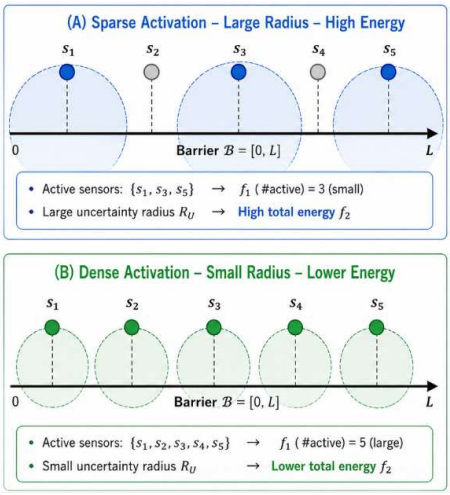
$$\text{s.t.} \quad I(x; \mathbf{u}, \mathbf{r}) \ge \gamma, \qquad \forall x \in \mathcal{B}, \tag{17b}$$

$$u_i \in \{0, 1\}, \qquad i = 1, 2, \ldots, N, \tag{17c}$$

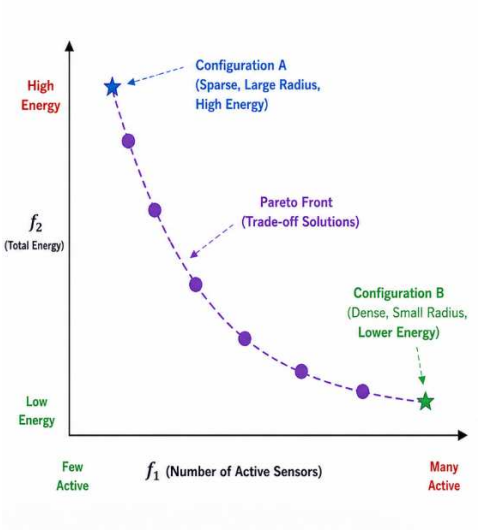
$$0 \le R_{U,i} \le R_U^{\max} u_i, \quad i = 1, 2, \ldots, N \tag{17d}$$

The output of B-PSBC is not a single solution but a Pareto set of feasible configurations. Each solution corresponds to a different compromise between sensor sparsity

and energy efficiency. In general, activating fewer sensors may require larger sensing radii to close coverage gaps, whereas activating more sensors may allow smaller individual radii and lower per-sensor energy consumption. This trade-off motivates the use of multi-objective optimization to approximate the Pareto front of B-PSBC.



(a) Sensor activation configurations in the decision space: sparse and dense activation patterns.



(b) Corresponding solutions mapped onto the Pareto front in the objective space.

Fig. 1: Illustration of the trade-off between the number of active sensors and total energy consumption in barrier coverage.

In the proposed RDC-MOEA framework, the evolutionary search is performed over the binary activation vector $\mathbf{u}$, while the corresponding radius vector $\mathbf{r}$ is constructed by a problem-specific radius decoder. This design decouples sensor selection from radius assignment and handles the feasibility of probabilistic strong barrier coverage through the decoding procedure.

5 The Proposed Radius-Decoder Multi-Objective Design

This section presents the proposed **Radius-Decoder-assisted Constrained Multi-Objective Evolutionary Algorithm**, abbreviated as **RDC-MOEA**, for solving the B-PSBC problem. The central idea is to separate the combinatorial sensor activation decision from the sensing-radius assignment. Instead of directly optimizing both the binary activation vector and the continuous uncertainty radii, RDC-MOEA evolves only the activation vector. For each activation pattern, a problem-specific decoder, called RadiusFormalize, constructs the corresponding radius vector and evaluates

the resulting objective values. This design has two advantages. First, it reduces the effective search space from a mixed binary–continuous space to a binary activation space. Second, it incorporates coverage feasibility handling into the decoding stage, thereby reducing the dependence on generic penalty or repair mechanisms. The evolutionary algorithm therefore, searches for promising activation structures, while the decoder determines the sensing radii required to satisfy the probabilistic strong barrier coverage condition whenever possible.

In this work, NSGA-II is adopted as the main evolutionary backbone of RDC-MOEA. The use of a dominance-based backbone is suitable for B-PSBC because the objective space is shaped by discrete activation decisions and nonlinear radius-dependent energy values. A small change in the activation vector may lead to a different decoded radius configuration and, consequently, a different energy–coverage trade-off. Figure 2 illustrates the overall workflow of RDC-MOEA.

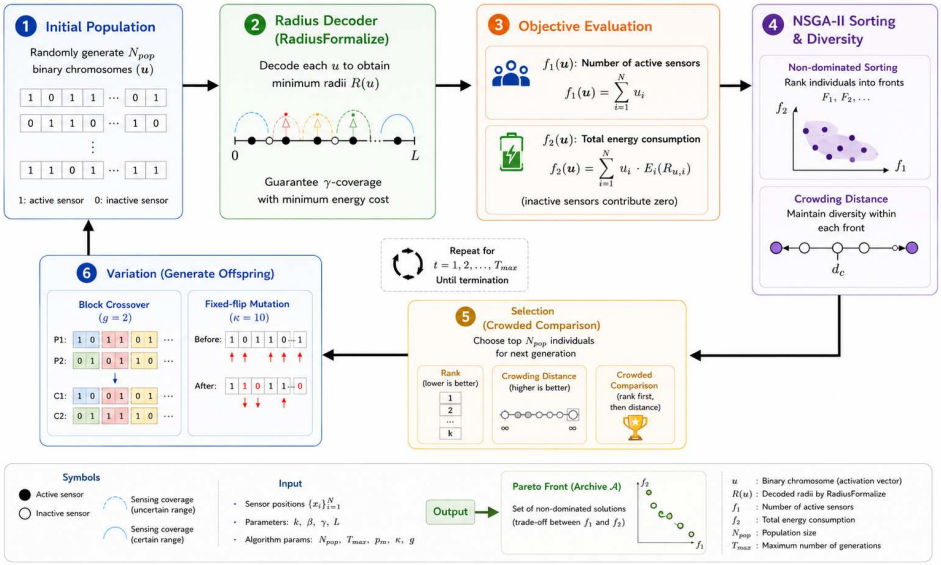


Fig. 2: Overall workflow of the proposed RDC-MOEA framework with the NSGA-II search backbone.

Although NSGA-II is used as the main implementation, the proposed radius-decoder-assisted design is not restricted to a single MOEA. To examine the influence of the search backbone, two additional variants are also implemented by replacing the NSGA-II search mechanism with MOEA/D and NSPSO, respectively. All variants use the same binary representation, the same RadiusFormalize decoder, and the same objective evaluation. Therefore, the comparison isolates the effect of the evolutionary search strategy under a common decoder-assisted framework. The main components of RDC-MOEA are summarized as follows: (1) a binary activation representation,

in which each chromosome specifies the set of active sensors; (2) the RadiusFormalize decoder, which assigns uncertainty radii to active sensors according to the barrier coverage requirement; (3) an NSGA-II-based evolutionary loop for maintaining a population of non-dominated activation patterns; and (4) block crossover and fixed-flip mutation operators designed for binary sensor activation patterns. Algorithm 1 presents the complete evolutionary loop of the NSGA-II-based RDC-MOEA.

Algorithm 1 NSGA-II-based RDC-MOEA for B-PSBC

Require: Sensor positions $\{x_i\}_{i=1}^{N}$; problem parameters $k, \beta, \gamma, L, R_U^{\max}$; algorithm parameters $N_{\text{pop}}, T_{\max}, p_m, n_{\text{flip}}, g$
Ensure: Final population $\mathcal{P}_{T_{\max}}$ as a Pareto-front approximation
Initialize a binary population $\mathcal{P}_0$ of size N_{pop}
for each $\mathbf{u} \in \mathcal{P}_0$ **do**
    $\mathbf{r} \leftarrow \textsc{RadiusFormalize}(\mathbf{u})$
    Evaluate $f_1(\mathbf{u})$ and $f_2(\mathbf{u}, \mathbf{r})$
end for each
Rank $\mathcal{P}_0$ using non-dominated sorting and crowding distance
for $t = 0$ **to** $T_{\max} - 1$ **do**
    Generate offspring population Q_t using block crossover and fixed-flip mutation
    for each $\mathbf{c} \in Q_t$ **do**
        $\mathbf{r} \leftarrow \textsc{RadiusFormalize}(\mathbf{c})$
        Evaluate $f_1(\mathbf{c})$ and $f_2(\mathbf{c}, \mathbf{r})$
    end for each
    $R_t \leftarrow \mathcal{P}_t \cup Q_t$
    Rank R_t using non-dominated sorting and crowding distance
    $\mathcal{P}_{t+1} \leftarrow \textsc{SelectTop}(R_t, N_{\text{pop}})$
end for
return $\mathcal{P}_{T_{\max}}$

5.1 Solution Representation and Population Initialization

Each candidate solution is represented by a binary chromosome

$$\mathbf{u} = (u_1, u_2, \ldots, u_N) \in \{0, 1\}^N, \tag{18}$$

where $u_i = 1$ indicates that sensor s_i is active and $u_i = 0$ indicates that it is inactive. The sensing radius is not encoded as an independent decision variable. Instead, for each chromosome $\mathbf{u}$, the radius vector

$$\mathbf{r} = (R_{U,1}, R_{U,2}, \ldots, R_{U,N}) \tag{19}$$

is generated by RadiusFormalize. Inactive sensors are assigned zero radius and do not contribute to the sensing intensity or energy consumption. After decoding, the two objective values are computed as defined in Section 4. The first objective counts

the number of active sensors, while the second objective evaluates the total energy consumption induced by the decoded radii. Thus, RDC-MOEA compares activation patterns according to their decoded coverage–energy behavior rather than their binary structure alone.

The initial population $\mathcal{P}_0$ is generated by random binary sampling. Each gene is independently drawn from a Bernoulli distribution:

$$u_i \sim \text{Bernoulli}(0.5), \qquad i = 1, 2, \ldots, N. \tag{20}$$

The all-zero chromosome is rejected because it cannot provide any barrier coverage. Each accepted chromosome is then decoded by RadiusFormalize and evaluated before the first generation begins.

5.2 Radius Formalization Decoder

The RadiusFormalize decoder is the core problem-specific component of RDC-MOEA. Given a binary activation vector $\mathbf{u}$, it assigns uncertainty detection radii to active sensors in a left-to-right manner along the barrier. The purpose of the decoder is to construct a radius configuration that satisfies the probabilistic strong barrier coverage requirement with low energy consumption. Since the energy function increases with the uncertainty radius, the decoder greedily searches for small valid radii for the selected active sensors. Let

$$\mathcal{A}(\mathbf{u}) = \{j \mid u_j = 1\} \tag{21}$$

be the active sensor set, and let

$$\mathcal{I} = [j_1, j_2, \ldots, j_m] \tag{22}$$

be the active indices sorted according to their positions on the barrier, i.e.,

$$x_{j_1} < x_{j_2} < \cdots < x_{j_m}. \tag{23}$$

The decoder proceeds in three main phases: handling the left boundary, assigning radii to interior sensor pairs, and checking the right boundary.

Boundary sensor handling. For the leftmost active sensor s_{j_1}, the decoder searches for the smallest uncertainty radius that allows the sensor to cover the left boundary $x = 0$ according to the sensing threshold γ. The same procedure is used for the rightmost active sensor by mirroring the coordinate system with right boundary $x = L$. Algorithm 2 describes this boundary handling procedure.

Algorithm 2 OUTERMOSTSENSOR(x, *isFirst*)

Require: Position x of the boundary sensor; flag *isFirst*
Ensure: Uncertainty radius for the boundary sensor

```
if isFirst = FALSE then
    x ← L − x
end if
R_U ← x
for r ← 1 to ⌈x⌉ do
    t ← x − (k − 1)r
    if exp(−βt) ≥ γ then
        R_U ← r
        break
    end if
end for
return ⌈R_U⌉
```

Interior sensor-pair handling. For each consecutive pair of active sensors $(s_{j_\ell}, s_{j_{\ell+1}})$, the decoder determines whether the already assigned radius of the left sensor is sufficient to cover the interval up to the right sensor. If the certain sensing region of s_{j_ℓ} already reaches $x_{j_{\ell+1}}$, then no additional radius is assigned to $s_{j_{\ell+1}}$ for this interval. Otherwise, the decoder first identifies the rightmost point x_{cer} that can still be sufficiently covered by the left sensor alone:

$$x_{\text{cer}} = \max\left\{x \le x_{j_{\ell+1}} \mid \exp\left[-\beta\left(x - x_{j_\ell} - (k-1)R_{U,j_\ell}\right)\right] \ge \gamma\right\}. \tag{24}$$

If $x_{\text{cer}} \ge x_{j_{\ell+1}}$, the interval is already covered by the left sensor. Otherwise, the decoder searches for a radius $R_{U,j_{\ell+1}}$ for the right sensor. For two adjacent sensors with different radii, the minimum combined sensing intensity over the interval occurs at the valley point

$$x^* = \frac{x_{j_\ell} + x_{j_{\ell+1}} - (k-1)\left(R_{U,j_\ell} - R_{U,j_{\ell+1}}\right)}{2}. \tag{25}$$

The candidate radius is accepted if the aggregate sensing intensity at x^* satisfies the threshold γ. The search range is bounded by

$$r_{\min} = \left\lceil \frac{x_{j_{\ell+1}} - x_{\text{cer}}}{k} \right\rceil, \qquad r_{\max} = \left\lceil \frac{x_{j_{\ell+1}} - x_{\text{cer}}}{k-1} \right\rceil. \tag{26}$$

Algorithm 3 gives the corresponding interior pair procedure.

Algorithm 3 InteriorSensorPair(ru_1, x_1, x_2)

Require: Left-sensor radius ru_1; left and right positions x_1, x_2
Ensure: Radius ru_2 for the right sensor

$r_1^{\mathrm{cer}} \leftarrow (k-1)ru_1$
if $x_1 + r_1^{\mathrm{cer}} \geq x_2$ **then**
    return 0
end if
$x_{\mathrm{cer}} \leftarrow x_2$
for $x \leftarrow \lceil x_1 + ru_1 \rceil$ **to** $\lceil x_2 \rceil$ **do**
    $t \leftarrow x - x_1 - r_1^{\mathrm{cer}}$
    if $\exp(-\beta t) \geq \gamma$ **then**
        $x_{\mathrm{cer}} \leftarrow x$
    end if
end for
if $x_{\mathrm{cer}} \geq x_2$ **then**
    return 0
end if
$ru_{2,\min} \leftarrow \lceil (x_2 - x_{\mathrm{cer}})/k \rceil$
$ru_{2,\max} \leftarrow \lceil (x_2 - x_{\mathrm{cer}})/(k-1) \rceil$
for $ru_2 \leftarrow ru_{2,\min}$ **to** $ru_{2,\max}$ **do**
    $r_2^{\mathrm{cer}} \leftarrow (k-1)ru_2$
    $x^* \leftarrow \lfloor x_1 + x_2 - (k-1)(ru_1 - ru_2) \rfloor / 2$
    $w \leftarrow \exp[-\beta(x^* - x_1 - r_1^{\mathrm{cer}})]$
      $+ \exp[-\beta(x_2 - x^* - r_2^{\mathrm{cer}})] - \gamma$
    if $w \geq 0$ **then**
        return ru_2
    end if
end for
return 0

Complete decoder. After all interior pairs have been processed, the decoder checks the rightmost active sensor against the right boundary $x = L$. If the boundary condition requires a larger radius than the one assigned during the interior-pair processing, the radius of the rightmost sensor is updated. Figure 3 illustrates the flow of RadiusFormalize, and Algorithm 4 gives the complete procedure.

Feasibility of the decoder. The RadiusFormalize decoder constructs the radius vector by processing active sensors from left to right. It covers the left boundary, repairs the gaps between adjacent active sensors, and finally checks the right boundary, while assigning zero radius to inactive sensors. To explain the feasibility of the adjacent-sensor repair step, consider two adjacent active sensors located at x_l and x_r, with uncertainty radii $R_{U,l}$ and $R_{U,r}$, respectively. For a point x between them, assume that both sensors contribute through their attenuation regions. The sensing

intensity at x is

$$I(x) = e^{-\beta\left(x-x_l-(k-1)R_{U,l}\right)} + e^{-\beta\left(x_r-x-(k-1)R_{U,r}\right)}. \tag{27}$$

Let

$$a(x) = x - x_l - (k-1)R_{U,l}, \quad \text{and} \quad b(x) = x_r - x - (k-1)R_{U,r}. \tag{28}$$

Then,

$$I(x) = e^{-\beta a(x)} + e^{-\beta b(x)}. \tag{29}$$

For fixed x_l, x_r, $R_{U,l}$, and $R_{U,r}$, we have

$$a(x) + b(x) = x_r - x_l - (k-1)(R_{U,l} + R_{U,r}) = D, \tag{30}$$

where D is constant. Therefore,

$$I(x) = e^{-\beta a(x)} + e^{-\beta(D-a(x))}. \tag{31}$$

By the arithmetic–geometric mean inequality,

$$e^{-\beta a(x)} + e^{-\beta b(x)} \geq 2\sqrt{e^{-\beta a(x)}e^{-\beta b(x)}} = 2e^{-\frac{\beta}{2}(a(x)+b(x))}. \tag{32}$$

Since $a(x) + b(x) = D$, we obtain

$$I(x) \geq 2e^{-\frac{\beta D}{2}}. \tag{33}$$

The equality holds when $a(x) = b(x)$. Solving this equation gives

$$x_w = \frac{x_l + x_r - (k-1)(R_{U,l} - R_{U,r})}{2}. \tag{34}$$

The decoder accepts a candidate radius $R_{U,r}$ for the right sensor only if the sensing intensity at this weakest point satisfies

$$I(x_w) \geq \gamma. \tag{35}$$

That is,

$$e^{-\beta\left(x_w-x_l-(k-1)R_{U,l}\right)} + e^{-\beta\left(x_r-x_w-(k-1)R_{U,r}\right)} \geq \gamma. \tag{36}$$

Therefore, if each adjacent pair of active sensors satisfies the above weakest-point condition, and the left and right boundary sensors are adjusted to cover the two endpoints of the barrier, then every point on the barrier is sufficiently covered. Hence, the radius vector produced by RadiusFormalize satisfies the probabilistic strong barrier coverage constraint.

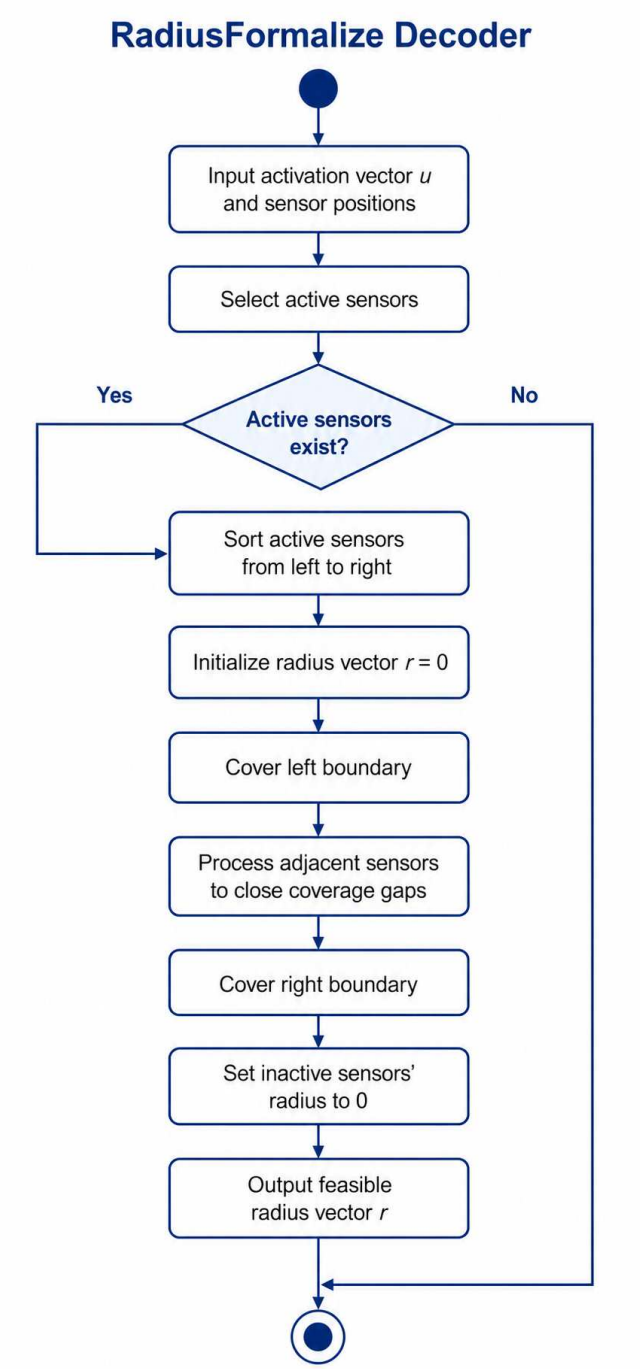


Fig. 3: Flowchart of the RadiusFormalize decoder.

Algorithm 4 RadiusFormalize($\mathbf{u}$)

Require: Binary activation vector $\mathbf{u}$; sensor positions $\{x_i\}_{i=1}^{N}$
Ensure: Radius vector $\mathbf{r}(\mathbf{u})$

$\mathcal{A} \leftarrow \{j \mid u_j = 1\}$
if $\mathcal{A} = \emptyset$ **then**
  return $(0, \ldots, 0)$
end if
$\mathcal{I} \leftarrow \text{sort}(\mathcal{A})$ by ascending x_j
$m \leftarrow |\mathcal{I}|$
$ru[1] \leftarrow \text{OutermostSensor}(x_{\mathcal{I}[1]}, \text{True})$
$z \leftarrow 0$
for $i \leftarrow 2$ **to** m **do**
  $\ell \leftarrow i - 1 - z$
  $r_{\text{tmp}} \leftarrow \text{InteriorSensorPair}(ru[\ell], x_{\mathcal{I}[\ell]}, x_{\mathcal{I}[i]})$
  if $r_{\text{tmp}} = 0$ **then**
    $z \leftarrow z + 1$
  else
    $z \leftarrow 0$
  end if
  $ru[i] \leftarrow r_{\text{tmp}}$
end for
$r_{\text{last}} \leftarrow \text{OutermostSensor}(x_{\mathcal{I}[m]}, \text{False})$
if $r_{\text{last}} > ru[m]$ **then**
  $ru[m] \leftarrow r_{\text{last}}$
end if
$\mathbf{r}(\mathbf{u}) \leftarrow (0, \ldots, 0)$
for $i \leftarrow 1$ **to** m **do**
  $r_{\mathcal{I}[i]} \leftarrow ru[i]$
end for
return $\mathbf{r}(\mathbf{u})$

5.3 Evolution Operators and Selection Mechanism

The proposed framework uses two binary variation operators: block crossover and fixed-flip mutation. These operators are designed for the activation-vector representation.

Block crossover

Block crossover partitions each chromosome into non-overlapping blocks of size g. For each block, the offspring inherits the block from one of the two parents with equal probability, while the second offspring receives the complementary block. Compared with uniform crossover, block crossover better preserves local co-activation patterns among neighboring sensors. This is useful because adjacent active sensors often jointly cover a local barrier segment.

Algorithm 5 BlockCrossover($\mathbf{u}^{(a)}, \mathbf{u}^{(b)}, g$)

Require: Parent chromosomes $\mathbf{u}^{(a)}, \mathbf{u}^{(b)}$; block size g
Ensure: Offspring chromosomes $\mathbf{c}^{(1)}, \mathbf{c}^{(2)}$
$\mathbf{c}^{(1)} \leftarrow [\,]$; $\mathbf{c}^{(2)} \leftarrow [\,]$
for $\ell \leftarrow 1, g+1, 2g+1, \ldots, N$ **do**
  $B_\ell \leftarrow \{\ell, \ell+1, \ldots, \min(\ell+g-1, N)\}$
  if Uniform$(0,1) > 0.5$ **then**
    Append $\mathbf{u}^{(a)}_{B_\ell}$ to $\mathbf{c}^{(1)}$; append $\mathbf{u}^{(b)}_{B_\ell}$ to $\mathbf{c}^{(2)}$
  else
    Append $\mathbf{u}^{(b)}_{B_\ell}$ to $\mathbf{c}^{(1)}$; append $\mathbf{u}^{(a)}_{B_\ell}$ to $\mathbf{c}^{(2)}$
  end if
end for
return $\mathbf{c}^{(1)}, \mathbf{c}^{(2)}$

Fixed-flip mutation

After crossover, each offspring undergoes mutation with probability p_m. When mutation is triggered, exactly n_{flip} bit positions are selected uniformly at random and flipped. This strategy provides a controlled perturbation level for binary activation patterns. In contrast to a per-locus mutation rate, the number of modified genes is explicitly controlled, which helps maintain exploration across different network sizes.

Algorithm 6 FixedFlipMutate($\mathbf{c}, n_{\text{flip}}$)

Require: Chromosome $\mathbf{c}$; number of flips n_{flip}
Ensure: Mutated chromosome $\mathbf{c}'$
$\mathbf{c}' \leftarrow \mathbf{c}$
for $t \leftarrow 1$ **to** n_{flip} **do**
  Draw $j \sim$ Uniform$\{1, 2, \ldots, N\}$
  $c'_j \leftarrow 1 - c'_j$
end for
return $\mathbf{c}'$

Selection

In the NSGA-II-based version of RDC-MOEA, population update is performed using non-dominated sorting and crowding-distance selection. At generation t, the parent population $\mathcal{P}_t$ and the offspring population Q_t are first combined into an intermediate population $R_t = \mathcal{P}_t \cup Q_t$. Each individual in R_t corresponds to a binary activation vector that has already been decoded by RadiusFormalize; therefore, its objective values are evaluated as the number of active sensors f_1 and the decoded energy consumption f_2. The individuals are then partitioned into a sequence of non-dominated fronts. The first front contains solutions that are not dominated by any other solution in R_t, while the subsequent fronts are obtained by repeatedly removing the previously identified fronts and extracting the next set of non-dominated solutions.

This ranking mechanism gives priority to activation patterns that provide better active-count–energy trade-offs.

After the non-dominated fronts are constructed, crowding distance is used to maintain diversity within each front. For each objective, the solutions in the same front are sorted according to their objective values, and the boundary solutions are assigned the largest crowding distance to preserve extreme trade-off points. For the remaining solutions, the crowding distance estimates how isolated a solution is from its neighboring solutions in the objective space. When two candidate solutions have the same non-domination rank, the one with the larger crowding distance is preferred, because it lies in a less crowded region of the approximated Pareto front. The next population $\mathcal{P}_{t+1}$ is obtained by selecting the best N_{pop} individuals from R_t according to this rank-and-diversity criterion. In RDC-MOEA, this selection mechanism allows decoded activation patterns to be compared directly in terms of their sparsity–energy trade-off, while preserving diverse configurations along the Pareto front.

5.4 Time Complexity Analysis

Let us remind that N denotes the number of deployed sensors, P is the population size, and G is the maximum number of generations. In RDC-MOEA, each individual is represented by a binary activation vector of length N. Therefore, the crossover and mutation operators require $\mathcal{O}(N)$ time for each generated offspring. The main problem-specific component is the RadiusFormalize decoder. Given a binary activation vector, the decoder first extracts and processes the active sensors from left to right. Let A be the number of active sensors, where $A \leq N$. For each active sensor pair, the decoder searches for the minimum feasible uncertainty radius according to the probabilistic coverage condition. If the barrier is discretized into B checking positions, the worst-case complexity of the decoding process is $\mathcal{O}(AB)$. Since $A \leq N$, the worst-case complexity of decoding one individual is $\mathcal{O}(NB)$. In the experimental setting of this paper, the barrier length is fixed, so this decoding cost behaves approximately linearly with respect to the number of sensors.

For each generation, RDC-MOEA evaluates P offspring. Thus, the total decoding and objective evaluation cost is $\mathcal{O}(PNB)$. In addition, the NSGA-II-based backbone performs non-dominated sorting and crowding-distance calculation. For two objectives, the fast non-dominated sorting procedure requires $\mathcal{O}(P^2)$ time, while crowding-distance sorting requires at most $\mathcal{O}(P \log P)$ time. Therefore, the total computational complexity of one generation is

$$\mathcal{O}(PNB + P^2 + P \log P). \tag{37}$$

Since $P \log P$ is dominated by P^2 in the NSGA-II selection procedure, the overall time complexity of RDC-MOEA over G generations can be written as

$$O\left(G(PNB + P^2)\right). \tag{38}$$

When the barrier discretization size B is fixed, the complexity can be simplified to

$$O\left(G(PN + P^2)\right). \tag{39}$$

This shows that the computational cost of RDC-MOEA mainly comes from two parts: the radius-decoding process used to ensure feasible barrier coverage, and the elitist non-dominated sorting mechanism used to maintain Pareto-front quality.

6 Experimental Evaluation

This section evaluates the performance of the proposed RDC-MOEA framework on the bi-objective probabilistic strong barrier coverage problem. The experiments are designed to examine three main aspects. First, we compare different multi-objective search backbones under the same radius-decoder-assisted representation. Second, we evaluate the contribution of the proposed RadiusFormalize decoder by comparing it with a common-radius decoding strategy. Third, we study the sensitivity of the algorithms to key sensing parameters, including the detection threshold, the attenuation coefficient, and the sensing-radius ratio.

6.1 Experimental Setup

6.1.1 Instance generation and parameters

The monitored barrier is modeled as a one-dimensional segment of length $L = 1000$. To evaluate scalability with respect to the number of deployed sensors, we consider five network sizes:

$$N \in \{100, 150, 200, 250, 300\}. \tag{40}$$

For each value of N, ten independent problem instances are randomly generated. In each instance, the sensor positions are sampled uniformly along the barrier, i.e.,

$$p_i \sim \mathcal{U}(0, L), \quad i = 1, 2, \ldots, N. \tag{41}$$

The same generated instances are used for all compared algorithms to ensure a fair comparison. Unless otherwise stated, the default sensing parameters are set to

$$(\gamma, \beta, k) = (0.5, 1.0, 2.0), \tag{42}$$

where γ is the required aggregate sensing-intensity threshold, β is the attenuation coefficient, and k controls the ratio between the maximum sensing radius and the uncertainty detection radius. The maximum uncertainty detection radius is set to $R_U^{\max} = 500$. These parameters define the default probabilistic strong barrier coverage setting used in the main comparison.

6.1.2 Compared algorithms

The main algorithm considered in this study is the NSGA-II-based implementation of the proposed radius-decoder-assisted framework, denoted as RDC-NSGA-II. In this

Table 1: Problem parameter settings.

Description	Value
Number of deployed sensors N	$\{100, 150, 200, 250, 300\}$
Barrier length L	1000
Sensor position p_i	$p_i \sim \mathcal{U}(0, L)$
Detection threshold γ	0.5
Attenuation coefficient β	1.0
Radius ratio parameter k	2.0
Maximum uncertainty detection radius $R_U^{\max}$	500

Table 2: Algorithm parameter settings for RDC-NSGA-II.

Parameter	Value
Population size	32
Maximum generations	10000
Number of runs per instance	10
Number of instances per N	10
Encoding scheme	Binary activation vector
Decoder	RadiusFormalize
Selection mechanism	Non-dominated sorting and crowding distance
Crossover operator	Block crossover
Mutation operator	Fixed-flip mutation

algorithm, each candidate solution is represented by a binary activation vector, and the corresponding uncertainty-radius vector is constructed by the proposed RadiusFormalize decoder. To examine the effect of the multi-objective search backbone, we compare RDC-NSGA-II with two representative evolutionary metaheuristics. These algorithms are selected because they represent decomposition-based and swarm-based multi-objective search strategies, respectively, and have been widely used for complex optimization problems in wireless sensor networks. The first variant replaces the NSGA-II search mechanism with MOEA/D [36, 39], resulting in an RDC-MOEA/D variant. The second variant replaces the search mechanism with NSPSO [37, 40], resulting in an RDC-NSPSO variant. All three variants use the same binary encoding, the same RadiusFormalize decoder, and the same objective evaluation procedure. Therefore, the comparison isolates the influence of the multi-objective search backbone under a common decoder-assisted framework.

In addition, to evaluate the contribution of the proposed decoder, we consider a Common-Radius NSGA-II ablation. This ablated variant uses the same NSGA-II backbone, population initialization, variation operators, and selection mechanism as RDC-NSGA-II. However, instead of assigning adaptive radii to active sensors through RadiusFormalize, it assigns the smallest feasible common uncertainty radius to all active sensors. This comparison isolates the effect of adaptive radius formalization from the effect of the evolutionary search backbone. The algorithmic parameters of RDC-NSGA-II are summarized in Table 2. The population size is fixed at 32, and each algorithm is executed for 10000 generations. For each problem instance, ten independent runs are performed and the results are reported on average.

6.1.3 Performance metrics and evaluation protocol

The algorithms are evaluated using three standard multi-objective performance indicators: Hypervolume (HV), Inverted Generational Distance (IGD), and Spread Delta. These metrics measure complementary aspects of the approximated Pareto fronts. HV measures the objective-space region dominated by the obtained non-dominated front with respect to a reference point. Since both objectives in B-PSBC are minimized, a larger HV value indicates a better combination of convergence and diversity. Meanwhile, IGD measures the average distance from a reference Pareto front to the front obtained by an algorithm. A smaller IGD value indicates that the obtained front is closer to the reference front and therefore provides a better approximation of the overall trade-off surface. Spread Delta evaluates the distribution uniformity of solutions along the obtained front. A smaller Spread Delta value indicates a more uniform distribution of non-dominated solutions, which is desirable because the output of B-PSBC is intended to provide multiple active-count–energy trade-off choices.

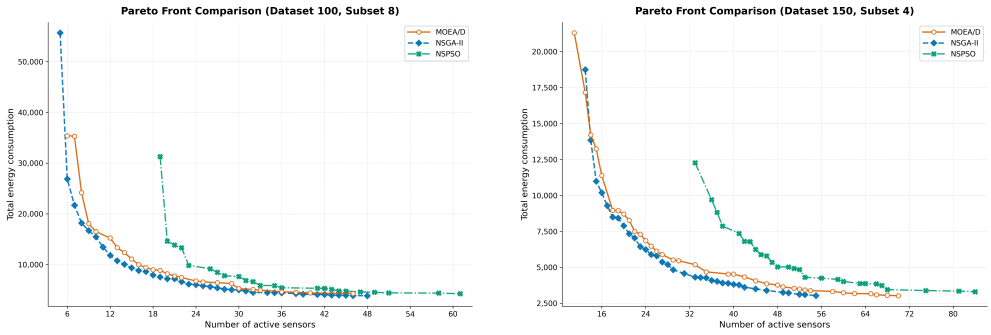
For each dataset size, the reported results are aggregated over all generated instances and independent runs. Specifically, for each value of N, ten independent problem instances are generated, and each algorithm is executed ten times on each instance. The final reported values are therefore computed over 100 runs for each dataset size and each algorithm. The same evaluation budget and the same problem instances are used for all compared algorithms. All algorithms were implemented in Python 3.8.10. The experiments were conducted on a server equipped with an Intel(R) Xeon(R) Gold 5220 CPU @ 2.20GHz with 12 logical CPUs, 31 GiB RAM, running Ubuntu 20.04.5 LTS. The source code was executed in a single-threaded setting, and no GPU acceleration was used in the reported experiments unless otherwise specified.

6.2 Overall Performance Comparison

This subsection compares MOEA/D, RDC-NSGA-II, and NSPSO under the default parameter setting $(\gamma, \beta, k) = (0.5, 1.0, 2.0)$. The two additional algorithms are selected as representative evolutionary metaheuristics for multi-objective optimization: MOEA/D represents a decomposition-based search strategy, whereas NSPSO represents a swarm-based search strategy. All three variants use the same binary encoding, the same RadiusFormalize decoder, and the same objective evaluation procedure. Therefore, the observed differences mainly reflect the effect of the multi-objective search backbone under a common decoder-assisted framework. The Common-Radius NSGA-II variant is introduced later in the ablation study to isolate the contribution of the proposed decoder.

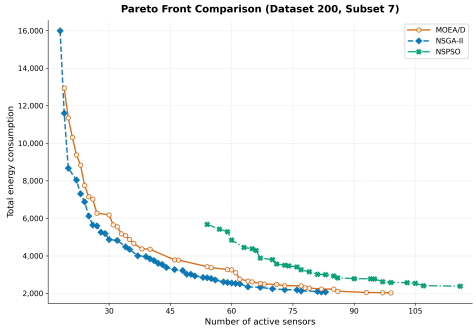
6.2.1 Pareto-front comparison

Figure 4 presents representative Pareto-front comparisons for five dataset sizes. The horizontal axis denotes the number of active sensors, and the vertical axis denotes the total energy consumption. Since both objectives are minimized, solutions closer to the lower-left region are preferred. The displayed fronts are used for visual inspection, while the overall conclusions are drawn from the aggregated HV, IGD, and Spread Delta results.

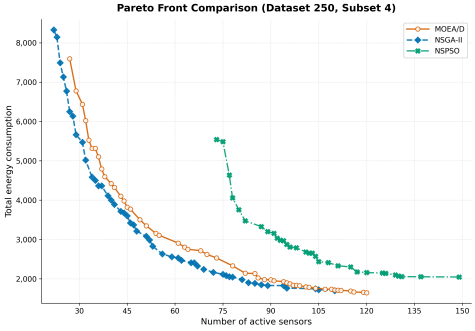


(a) $N = 100$

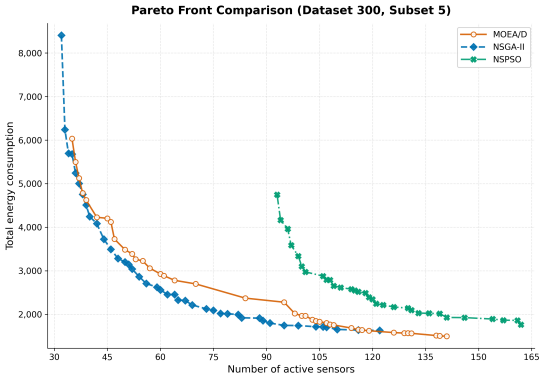
(b) $N = 150$



(c) $N = 200$



(d) $N = 250$



(e) $N = 300$

Fig. 4: Pareto front comparison of MOEA/D, RDC-NSGA-II, and NSPSO under the default parameter setting $(\gamma, \beta, k) = (0.5, 1.0, 2.0)$.

Across the five problem sizes, RDC-NSGA-II generally provides fronts that are closer to the low-energy region and better distributed along the trade-off surface. MOEA/D remains competitive, particularly on smaller datasets, but its distribution becomes less stable as N increases. NSPSO produces weaker fronts in most cases, with solutions farther from the desirable lower-left region and a less uniform spread. These observations suggest that dominance-based elitist selection is well suited to the discrete activation space and the discontinuous changes introduced by the radius decoder.

6.2.2 HV and IGD results

Table 3 reports the final HV values for all dataset sizes. RDC-NSGA-II achieves the highest HV in every case, indicating the best overall balance between convergence and diversity. MOEA/D consistently ranks second and remains a competitive alternative, whereas NSPSO obtains substantially lower HV values. The gap between NSPSO and the two evolutionary variants becomes more evident as the number of deployed sensors increases.

Table 3: Hypervolume comparison over different dataset sizes.

Dataset size	MOEA/D	RDC-NSGA-II **(ours)**	NSPSO
100	0.703326 ± 0.072526	**0.718266 ± 0.068777**	0.529123 ± 0.034595
150	0.633701 ± 0.062408	**0.657400 ± 0.053920**	0.420688 ± 0.032218
200	0.590802 ± 0.052805	**0.619541 ± 0.047214**	0.354290 ± 0.027225
250	0.538362 ± 0.050244	**0.572403 ± 0.052494**	0.299584 ± 0.024791
300	0.521512 ± 0.046340	**0.538206 ± 0.050851**	0.266975 ± 0.025462

Table 4 reports the IGD results. RDC-NSGA-II obtains the lowest IGD for all dataset sizes, meaning that its approximated fronts are closest to the empirical reference fronts. MOEA/D is consistently the second-best method, while NSPSO has much larger IGD values. As N increases, the IGD values of all methods tend to increase, but RDC-NSGA-II maintains the smallest degradation, indicating better robustness to the increasing dimension of the activation vector.

Table 4: IGD comparison over different dataset sizes.

Dataset size	MOEA/D	RDC-NSGA-II **(ours)**	NSPSO
100	0.068588 ± 0.017160	**0.044439 ± 0.014157**	0.147440 ± 0.024847
150	0.071985 ± 0.015208	**0.049026 ± 0.014167**	0.218045 ± 0.022777
200	0.075134 ± 0.014781	**0.055096 ± 0.014800**	0.242904 ± 0.025407
250	0.084627 ± 0.017056	**0.061657 ± 0.017862**	0.292863 ± 0.028053
300	0.086036 ± 0.016655	**0.065244 ± 0.016348**	0.299753 ± 0.032322

Figure 5 provides a visual comparison of the mean IGD values. The figure confirms the same ranking observed in Table 4: RDC-NSGA-II achieves the best approximation

quality, followed by MOEA/D, while NSPSO remains clearly less competitive under the same decoder-assisted representation.

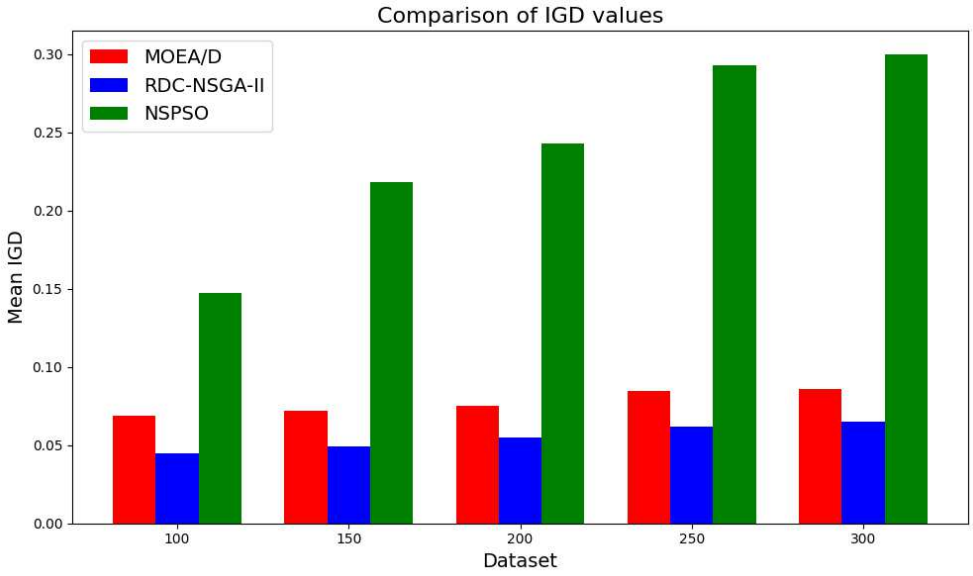
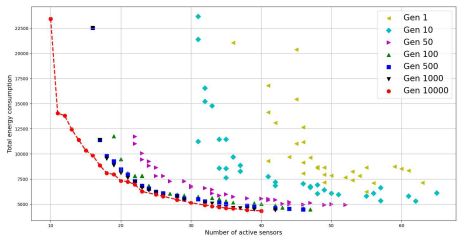


Fig. 5: Comparison of IGD values for MOEA/D, RDC-NSGA-II, and NSPSO under the default parameter setting.

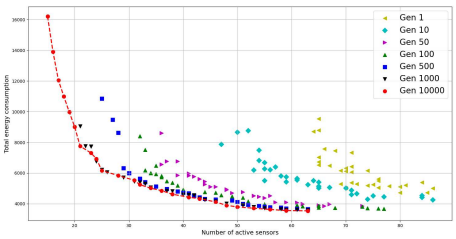
6.2.3 Convergence behavior

Before reporting the quantitative convergence comparison among the three algorithms, Figure 6 illustrates the evolutionary behavior of RDC-NSGA-II over different generations. The horizontal axis denotes the number of active sensors, while the vertical axis denotes the total energy consumption. Since both objectives are minimized, the desirable search direction is toward the lower-left region. Across all dataset sizes, the population gradually moves from scattered high-cost solutions in the early generations to more compact and competitive trade-off fronts in later generations. This observation indicates that the proposed radius-decoder-assisted search can progressively improve both objectives while maintaining a diverse set of non-dominated solutions.

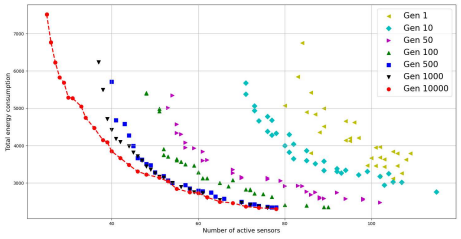
Figure 7 further compares the HV convergence behavior of MOEA/D, RDC-NSGA-II, and NSPSO under the same default parameter setting. RDC-NSGA-II and MOEA/D converge to clearly higher HV values than NSPSO. Among them, RDC-NSGA-II obtains the best final HV, showing that non-dominated sorting combined with crowding-distance preservation is effective for maintaining high-quality trade-off solutions under the proposed decoder. The convergence curves also indicate that RDC-NSGA-II can continuously improve the quality of the approximated Pareto front throughout the evolutionary process.



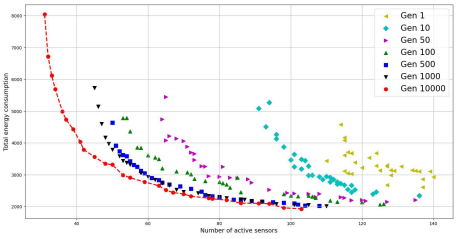
(a) $N = 100$



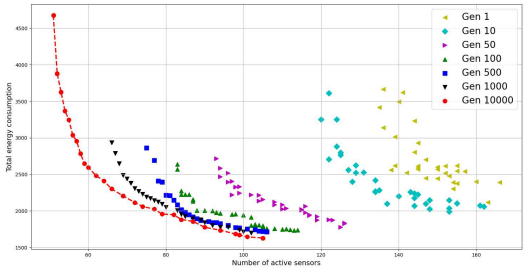
(b) $N = 150$



(c) $N = 200$



(d) $N = 250$



(e) $N = 300$

Fig. 6: Evolution of the RDC-NSGA-II population over different generations.

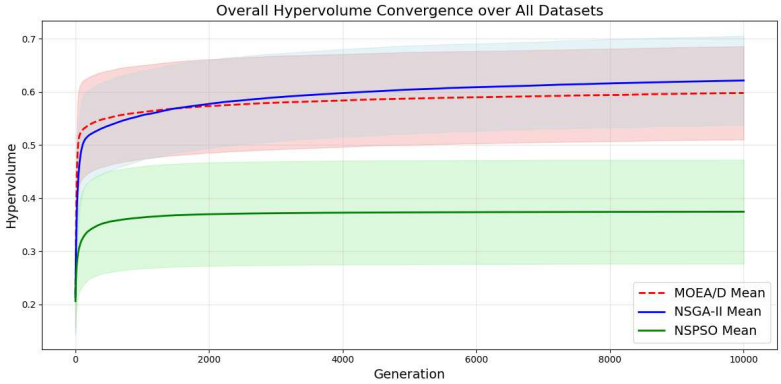
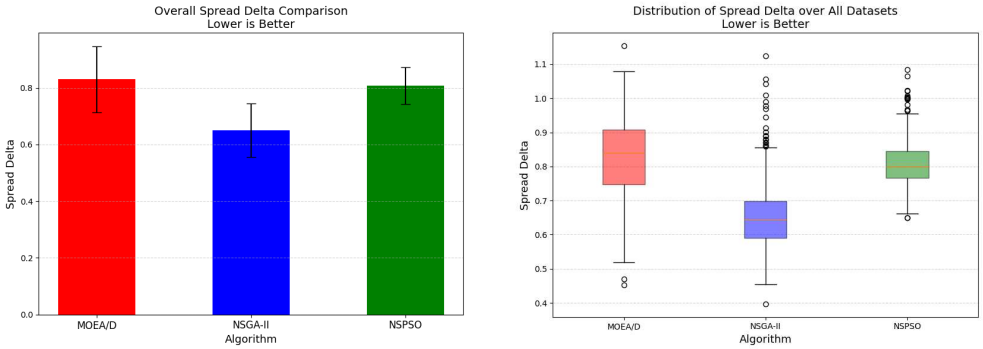


Fig. 7: HV convergence curves of MOEA/D, RDC-NSGA-II, and NSPSO.

6.2.4 Diversity analysis

Figure 8 evaluates the distribution uniformity of the obtained fronts. RDC-NSGA-II achieves the lowest average Spread Delta and the lowest median value in the boxplot, indicating a more uniform distribution of solutions along the Pareto front. These results complement the HV and IGD analyses by showing that RDC-NSGA-II improves not only approximation quality but also solution spread.



(a) Overall comparison.

(b) Distribution over all datasets.

Fig. 8: Spread Delta comparison of MOEA/D, RDC-NSGA-II, and NSPSO under the default parameter setting.

Overall, the three indicators lead to the same conclusion. RDC-NSGA-II provides the best overall performance among the compared variants, with the highest HV, the lowest IGD, and the most uniform solution distribution. MOEA/D remains competitive but is less consistent in preserving both convergence and diversity. NSPSO performs the weakest in this setting, likely because swarm-based dynamics are less effective in the binary activation space coupled with radius-decoder-induced discontinuities.

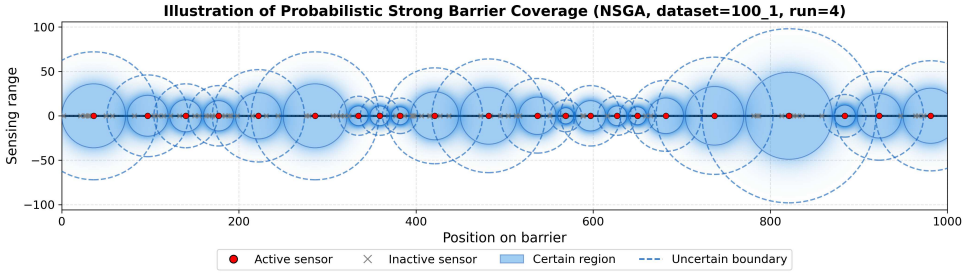
6.3 Ablation Study: Effect of RadiusFormalize

This subsection evaluates the contribution of the proposed RadiusFormalize decoder. To isolate the effect of the decoder from the effect of the evolutionary search backbone, we construct an ablated variant called Common-Radius NSGA-II. This variant uses the same NSGA-II backbone as RDC-NSGA-II, including the same population size, initialization scheme, crossover operator, mutation operator, selection mechanism, and objective evaluation procedure. The only difference lies in the decoding step. RDC-NSGA-II assigns individually adapted uncertainty radii to active sensors through RadiusFormalize, whereas Common-Radius NSGA-II assigns the smallest feasible common uncertainty radius to all active sensors. Therefore, this ablation directly examines whether adaptive radius formalization improves the quality of the obtained active-count–energy trade-off fronts.

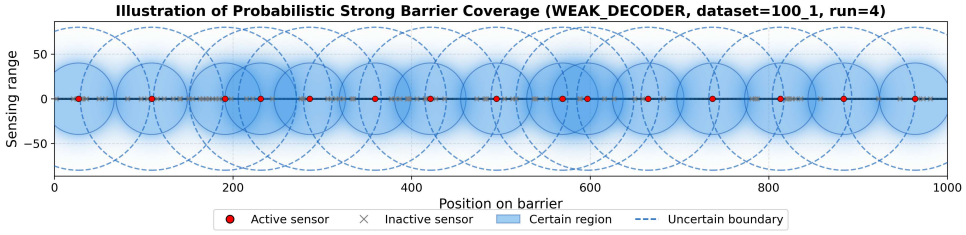
6.3.1 Qualitative comparison of decoded coverage

Figure 9 illustrates the qualitative difference between the two decoding strategies on a representative instance. RDC-NSGA-II with RadiusFormalize produces non-uniform sensing radii that adapt to local sensor spacing along the barrier. Sensors located in sparse regions can be assigned larger radii when necessary, while sensors in dense regions can use smaller radii to avoid unnecessary energy consumption. In contrast, the common-radius decoder applies the same uncertainty radius to all active sensors, regardless of the local deployment density.

This difference is important for the B-PSBC problem because the energy objective is directly determined by the decoded radii. A common-radius assignment may satisfy the coverage constraint, but it tends to allocate sensing effort uniformly even when local coverage conditions are heterogeneous. As a result, it may introduce unnecessary energy consumption in well-covered regions. By contrast, RadiusFormalize exploits the spatial structure of the barrier and constructs a more flexible radius configuration. This allows the evolutionary search to evaluate each activation pattern according to a more energy-aware and locally adapted coverage configuration.



(a) RDC-NSGA-II with RadiusFormalize.



(b) Common-Radius decoder.

Fig. 9: Illustration of the coverage configurations produced by the two decoder strategies on a representative instance.

6.3.2 Pareto-front comparison with common-radius decoding

Figure 10 compares the Pareto fronts obtained by RDC-NSGA-II and Common-Radius NSGA-II on a representative instance with $N = 100$. Since both variants use the same NSGA-II backbone, the difference between the two fronts mainly reflects the effect of the decoding strategy. The front obtained by RDC-NSGA-II is located closer to the desirable lower-left region, especially in the low-energy part of the objective space. This indicates that adaptive radius assignment helps the search process discover more competitive feasible solutions.

The improvement can be explained by the fact that RadiusFormalize adapts the sensing radius of each active sensor to the local coverage requirement. For the same or a similar number of active sensors, the proposed decoder can reduce unnecessary radius inflation and hence reduce total energy consumption. In contrast, the common-radius strategy is less flexible because all active sensors must share the same uncertainty radius. This makes it more difficult to obtain fine-grained trade-offs between the number of active sensors and the total energy consumption.

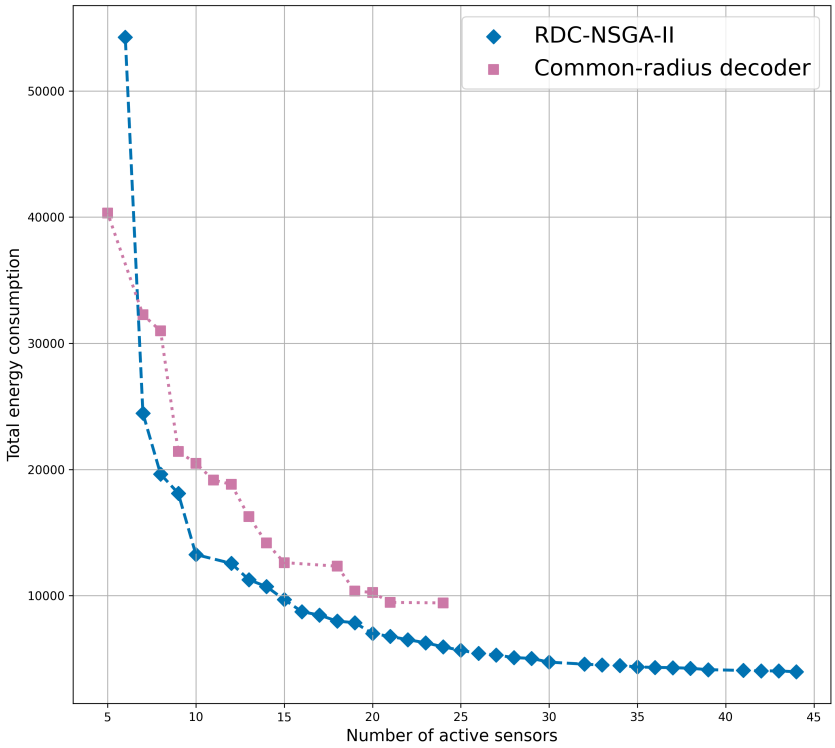


Fig. 10: Pareto-front comparison between RDC-NSGA-II and the common-radius ablation for a representative instance with $N = 100$.

6.3.3 Quantitative HV and IGD ablation

Table 5 reports the HV results of RDC-NSGA-II and Common-Radius NSGA-II. A common instance-wise normalization is used so that both variants are evaluated in the same objective space. RDC-NSGA-II achieves higher mean HV values for all dataset sizes, showing that RadiusFormalize improves the overall quality of the obtained Pareto-front approximation. The advantage becomes more pronounced as the problem size increases. For example, when $N = 300$, RDC-NSGA-II obtains an HV value of 0.998635, whereas Common-Radius NSGA-II obtains 0.667610. This result suggests that adaptive radius decoding becomes increasingly important in larger deployments, where local sensor spacing is more heterogeneous and a uniform-radius assignment becomes less effective.

Table 5: Decoder ablation based on HV, where a larger value is better.

N	RDC-NSGA-II	Common-Radius NSGA-II
100	1.017560 ± 0.047025	0.981059 ± 0.089965
150	1.006544 ± 0.048040	0.903172 ± 0.128089
200	1.048936 ± 0.043269	0.934414 ± 0.110401
250	1.022300 ± 0.051212	0.874116 ± 0.191044
300	0.998635 ± 0.055103	0.667610 ± 0.305261

Table 6 gives the corresponding IGD results. RDC-NSGA-II consistently obtains lower IGD values than Common-Radius NSGA-II across all dataset sizes, indicating that its obtained fronts are closer to the reference fronts. The performance gap also increases with N. At $N = 300$, the IGD of RDC-NSGA-II is 0.069556, while that of Common-Radius NSGA-II is 0.447036. This confirms that common-radius decoding becomes less reliable as the network size grows.

Table 6: Decoder ablation based on IGD, where a smaller value is better.

N	RDC-NSGA-II	Common-Radius NSGA-II
100	0.048574 ± 0.012865	0.209034 ± 0.057149
150	0.055022 ± 0.016505	0.245988 ± 0.059218
200	0.061425 ± 0.014071	0.253345 ± 0.053877
250	0.069736 ± 0.019949	0.322297 ± 0.091351
300	0.069556 ± 0.016439	0.447036 ± 0.171951

Overall, the ablation study confirms that RadiusFormalize is a key component of the proposed framework. Although RDC-NSGA-II and Common-Radius NSGA-II use the same evolutionary search mechanism, replacing adaptive radius formalization with a common-radius decoding strategy leads to clear degradation in both HV and

IGD. These results demonstrate that the performance gain of RDC-NSGA-II does not come only from the NSGA-II backbone, but also from problem-specific decoder that transforms each activation pattern into a locally adapted and energy-aware configuration.

6.4 Robustness to Sensing Parameters

This subsection evaluates the robustness of the compared algorithms under different sensing conditions. The probabilistic strong barrier coverage constraint is directly affected by three key parameters: the detection threshold γ, the attenuation coefficient β, and the sensing-radius ratio k. The detection threshold γ determines the minimum aggregate sensing intensity required at every barrier point. The attenuation coefficient β controls how quickly the sensing contribution decays in the uncertainty region. The radius ratio k determines the relationship between the uncertainty detection radius and the maximum sensing radius. Varying these parameters changes the difficulty of the B-PSBC problem and allows us to examine whether the relative performance of RDC-NSGA-II remains stable under different coverage requirements. We use heatmaps to visualize the sensitivity results. In each figure, the upper row reports HV, where a larger value is better, and the lower row reports IGD, where a smaller value is better. The three columns correspond to MOEA/D, RDC-NSGA-II, and NSPSO, respectively. Each cell represents the result for one pair of dataset size and sensing-parameter value.

6.4.1 Effect of detection threshold

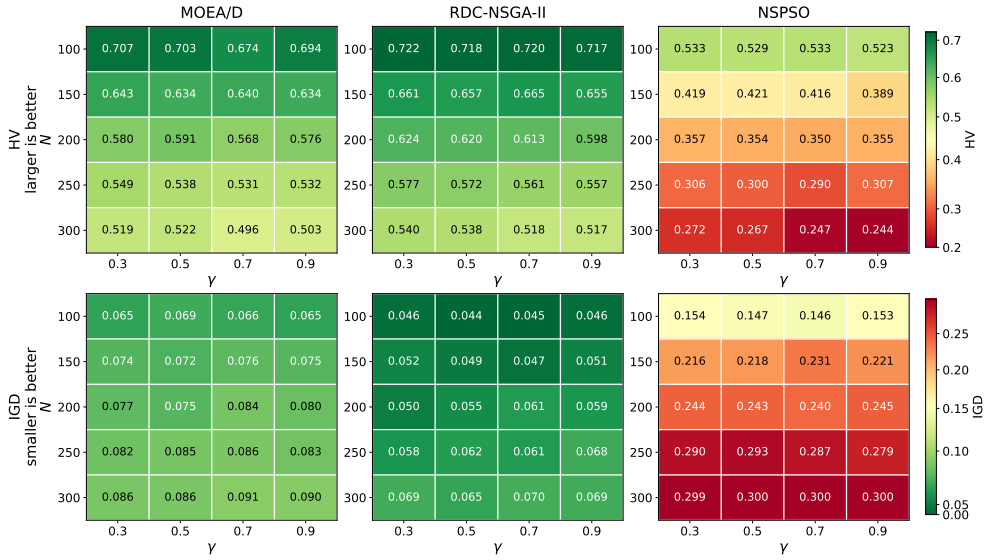


Fig. 11: Sensitivity analysis with respect to the detection threshold γ, where $\beta = 1.0$ and $k = 2.0$. The upper row reports HV and the lower row reports IGD.

The detection threshold γ defines the required minimum aggregate sensing intensity at each point on the barrier. A larger γ imposes a stricter probabilistic coverage requirement and may require either more active sensors, larger sensing radii, or both. In this experiment, γ is varied in $\{0.3, 0.5, 0.7, 0.9\}$, while $\beta = 1.0$ and $k = 2.0$ are fixed. Figure 11 shows the sensitivity results with respect to γ. Across all tested threshold values and dataset sizes, RDC-NSGA-II consistently achieves the highest HV among the three algorithms. This indicates that the proposed method maintains the best overall balance between convergence and diversity even when the coverage requirement becomes stricter. MOEA/D remains the second-best method in most cases, while NSPSO produces clearly lower HV values, especially for larger datasets. The IGD results lead to the same conclusion. RDC-NSGA-II obtains the lowest IGD across the tested configurations, showing that its approximated fronts remain closest to the reference fronts. As the dataset size increases, the IGD values generally become larger, which is expected because the binary activation vector becomes higher-dimensional and the search space becomes more complex. Nevertheless, the relative ranking of the algorithms remains stable. These results show that RDC-NSGA-II is robust to different detection-threshold settings and is not sensitive to a particular choice of γ.

6.4.2 Effect of attenuation coefficient

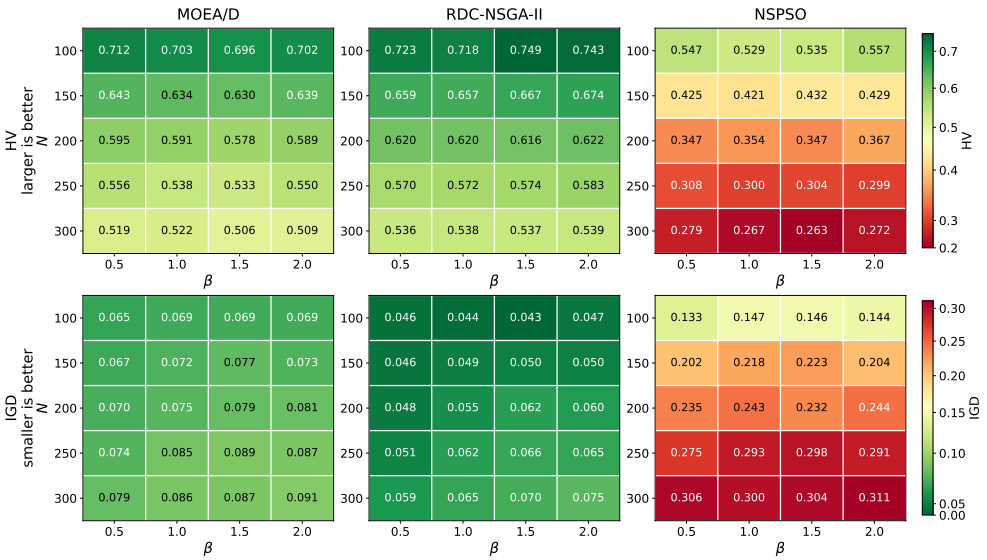


Fig. 12: Sensitivity analysis with respect to the attenuation coefficient β, where $\gamma = 0.5$ and $k = 2.0$. The upper row reports HV and the lower row reports IGD.

The attenuation coefficient β controls the decay rate of the sensing contribution in the uncertainty region. A larger β means that the sensing contribution decreases more rapidly with distance, making it more difficult for distant sensors to jointly cover

weakly monitored barrier points. In this experiment, β is varied in $\{0.5, 1.0, 1.5, 2.0\}$, while $\gamma = 0.5$ and $k = 2.0$ are fixed. Figure 12 reports the corresponding HV and IGD results. RDC-NSGA-II achieves the highest HV in all tested configurations. The HV values remain relatively stable when β changes, suggesting that the proposed decoder-assisted search can adapt to different attenuation conditions. This stability is important because the attenuation coefficient reflects environmental uncertainty and sensing degradation, which may vary across practical deployment scenarios. For IGD, RDC-NSGA-II again obtains the best results across all dataset sizes and all values of β. Although the IGD values tend to increase slightly when β becomes larger, the degradation is moderate compared with the gap between RDC-NSGA-II and the other two algorithms. MOEA/D remains competitive but generally produces higher IGD values, while NSPSO is consistently less accurate. These observations indicate that the proposed framework remains effective even when the sensing signal decays faster in the uncertainty region.

6.4.3 Effect of radius ratio

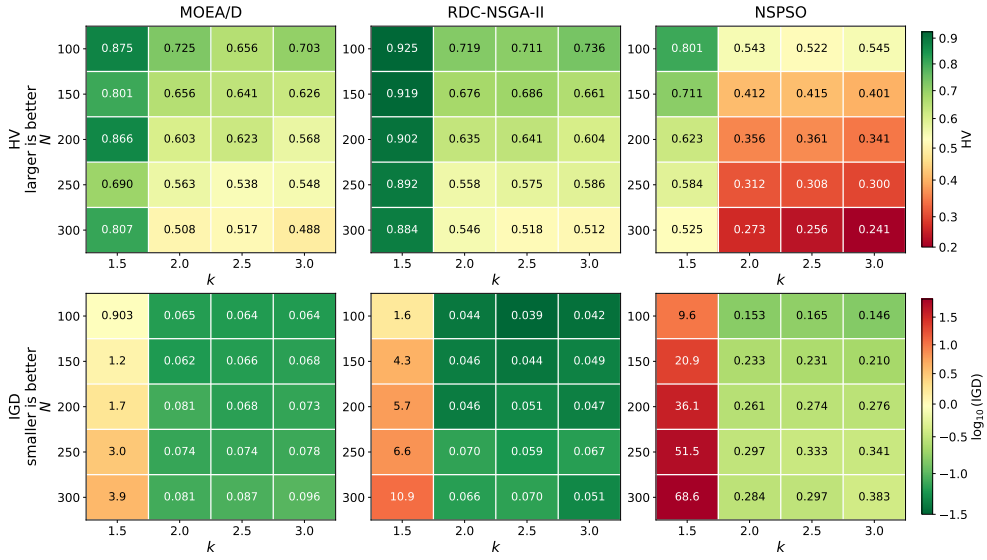


Fig. 13: Sensitivity analysis with respect to the radius ratio k, where $\gamma = 0.5$ and $\beta = 1.0$. The upper row reports HV and the lower row reports IGD. The color scale of IGD is based on $\log_{10}$(IGD) for better visualization, while the cell annotations show the original IGD values.

The radius ratio k determines the relationship between the uncertainty detection radius and the maximum sensing radius. A smaller k restricts the effective sensing range associated with each uncertainty radius and can make the coverage constraint more difficult to satisfy. Conversely, a larger k expands the maximum sensing range

and may provide more flexibility for constructing feasible barrier coverage. In this experiment, k is varied in $\{1.5, 2.0, 2.5, 3.0\}$, while $\gamma = 0.5$ and $\beta = 1.0$ are fixed. Figure 13 shows that the setting $k = 1.5$ is substantially different from the other settings. Under this restrictive sensing range, the HV values are generally higher because the objective-space scale and the feasible trade-off structure are changed. RDC-NSGA-II achieves the best HV for all dataset sizes at $k = 1.5$, indicating that the proposed decoder-assisted dominance-based search is effective in preserving high-quality trade-off solutions under a restrictive sensing-range condition. For $k \geq 2.0$, RDC-NSGA-II remains the best or highly competitive in terms of HV across most dataset sizes, while NSPSO consistently obtains the lowest HV. When $k = 1.5$, MOEA/D obtains lower IGD than RDC-NSGA-II. This suggests that decomposition-based search can approximate the reference front more closely under the most restrictive sensing-range setting. However, this behavior is limited to the extreme case $k = 1.5$. For all tested dataset sizes with $k \geq 2.0$, RDC-NSGA-II achieves the lowest IGD. Therefore, once the sensing range is not overly restrictive, the dominance-based selection and crowding-distance preservation of RDC-NSGA-II provide a more accurate and stable approximation of the Pareto front.

7 Conclusions

This paper proposed RDC-MOEA, a radius-decoder-assisted constrained multi-objective evolutionary framework for the bi-objective probabilistic strong barrier coverage problem in wireless sensor networks. Instead of directly optimizing both binary sensor activation decisions and continuous sensing radii, the proposed framework evolves binary activation patterns and uses the problem-specific RadiusFormalize decoder to construct the corresponding sensing-radius configurations. This design reduces the effective search space and incorporates coverage-feasibility handling into the decoding process. Three decoder-assisted variants based on NSGA-II, MOEA/D, and NSPSO were evaluated under the same experimental setting. The results show that the NSGA-II-based RDC-MOEA achieves the best overall performance, obtaining higher Hypervolume, lower IGD, and better Spread Delta values across the tested instances. These results indicate that dominance-based elitist selection with crowding-distance preservation is well suited to the binary activation space induced by the proposed decoder. MOEA/D remains a competitive alternative, while NSPSO is less effective in this decoder-assisted setting. The ablation study further confirms the importance of RadiusFormalize: replacing it with a common-radius decoder leads to clear degradation in both HV and IGD. The sensitivity analysis also shows that RDC-NSGA-II remains robust under different detection thresholds, attenuation coefficients, and sensing-radius ratios, although MOEA/D can be advantageous in terms of IGD under the most restrictive radius-ratio setting. In future work, we will investigate more advanced radius decoders, adaptive variation operators, and hybrid evolutionary strategies to further improve scalability, convergence speed, and diversity preservation. We also plan to extend the proposed framework to more complex WSN deployment scenarios, including heterogeneous sensors, connectivity constraints, dynamic energy models, and two-dimensional or obstacle-aware barrier coverage settings.

References

[1] Trigka, M., Dritsas, E.: Wireless sensor networks: From fundamentals and applications to innovations and future trends. IEEE Access **13**, 96365–96399 (2025) https://doi.org/10.1109/ACCESS.2025.3572328

[2] Gulati, K., Boddu, R.S.K., Kapila, D., Bangare, S.L., Chandnani, N., Saravanan, G.: A review paper on wireless sensor network techniques in Internet of Things (IoT). Materials Today: Proceedings **51**, 161–165 (2021) https://doi.org/10.1016/j.matpr.2021.05.067

[3] Binh, N.T.M., Luong, H.V.D., Tuan, N.D., Duan, L.V., Binh, H.T.T.: A hybrid GA–PSO with collective learning for obstacle-aware sensor node deployment in IoT-enabled networks. In: Proceedings of the Genetic and Evolutionary Computation Conference (2026). https://doi.org/10.1145/3795095.3805074 . https://doi.org/10.1145/3795095.3805074

[4] Chowdhury, S.M., Hossain, A.: Different energy saving schemes in wireless sensor networks: A survey. Wireless Personal Communications **114**(3), 2043–2062 (2020) https://doi.org/10.1007/s11277-020-07461-5

[5] M. Al-Qurabat, A.K., Abdulhussein Abdulzahra, S.: An overview of periodic wireless sensor networks to the Internet of Things. In: IOP Conference Series: Materials Science and Engineering, vol. 928, p. 032055 (2020). https://doi.org/10.1088/1757-899X/928/3/032055 . IOP Publishing

[6] Shaikh, M.S., Wang, C., Xie, S., Zheng, G., Dong, X., Qiu, S., Ahmad, M.A., Raj, S.: Coverage and connectivity maximization for wireless sensor networks using improved chaotic grey wolf optimization. Scientific Reports **15**(1), 15706 (2025) https://doi.org/10.1038/s41598-025-00184-2

[7] Moslehi, M.M.: Exploring coverage and security challenges in wireless sensor networks: A survey. Computer networks **260**, 111096 (2025) https://doi.org/10.1016/j.comnet.2025.111096

[8] Thi My Binh, N., Son Tung, T., Dung, T.L., Duc Luong, H.V.: Maximizing lifetime and target coverage in dynamic underwater wireless sensor networks using an enhanced genetic algorithm. Journal of Network and Systems Management **34**(4), 108 (2026) https://doi.org/10.1007/s10922-026-10080-3

[9] Binh, N.T.M., Binh, H.T.T., Luong, H.V.D., Long, N.T., Van Chien, T.: An efficient exact method with polynomial time-complexity to achieve k-strong barrier coverage in heterogeneous wireless multimedia sensor networks. Journal of Network and Computer Applications **231**, 103985 (2024) https://doi.org/10.1016/j.jnca.2024.103985

[10] Suganthi, S., Umapathi, N., Venkateswaran, N., Rajarajan, S.: Enhancing energy

efficiency in wireless sensor networks via predictive model for node status classification and coverage integrity using relational Bi-level aggregation graph convolutional network. Expert Systems with Applications **296**, 129029 (2025) https://doi.org/10.1016/j.eswa.2025.129029

[11] Binh, N.T.M., Luong, H.V.D., Anh, M.D.Q., Khanh, L.N.: An efficient discretization and transformation scheme for maximizing secure lifetime problem in heterogeneous wireless rotatable camera sensor networks with barrier coverage. Cluster Computing **28**(6), 374 (2025) https://doi.org/10.1007/s10586-025-05165-8

[12] Elhabyan, R., Shi, W., St-Hilaire, M.: Coverage protocols for wireless sensor networks: Review and future directions. Journal of Communications and Networks **21**(1), 45–60 (2019) https://doi.org/10.1109/JCN.2019.000005

[13] Van Son, N., Hanh, N.T., Minh, T.T., Binh, H.T.T., Thang, N.X.: Heuristic and approximate Steiner tree algorithms for ensuring network connectivity in mobile wireless sensor networks. Journal of Network and Computer Applications **238**, 104155 (2025) https://doi.org/10.1016/j.jnca.2025.104155

[14] Kumar, S.P., Nagendranath, M., Alsamri, J., Ebad, S.A.: Enhanced deep learning-based optimization model for the coverage optimization in wireless sensor networks. International Journal of Computational Intelligence Systems **18**(1), 83 (2025) https://doi.org/10.1007/s44196-025-00803-w

[15] Masum, M.H., Raj, B., Showmik, S.S.: Toward efficient and accurate anomaly detection in wireless sensor networks: A review. IEEE Sensors Journal **25**(24), 43585–43602 (2025) https://doi.org/10.1109/JSEN.2025.3618906

[16] Mohamed, R.E., Saleh, A.I., Abdelrazzak, M., Samra, A.S.: Survey on wireless sensor network applications and energy efficient routing protocols. Wireless Personal Communications **101**(2), 1019–1055 (2018) https://doi.org/10.1007/s11277-018-5747-9

[17] Binh, N.T.M., Vu, L.D.A., Viet, N.H., Binh, H.T.T., Luong, H.V.D.: Extending network lifespan and securing effective barrier coverage in 3D underwater wireless sensor networks. Cluster Computing **29** (2026) https://doi.org/10.1007/s10586-026-06113-w

[18] Amutha, J., Sharma, S., Nagar, J.: WSN strategies based on sensors, deployment, sensing models, coverage and energy efficiency: Review, approaches and open issues. Wireless Personal Communications **111**(2), 1089–1115 (2019)

[19] Phan Duc, H., Bui Trong, D., Nguyen Thi, T., Huynh Thi Thanh, B.: Pareto front grid guided multiobjective optimization in dynamic pickup and delivery problem considering two-sided fairness. In: Proceedings of the Genetic and Evolutionary Computation Conference, pp. 277–285. Association for Computing Machinery, ??? (2025). https://doi.org/10.1145/3712256.3726467

[20] Duc, B.T., Chien, T.V., Ngo, H.Q., Binh, H.T.T.: Multi-objective signal optimization to balance multiple conflicting metrics in RIS-assisted MIMO systems. In: Proceedings of the Genetic and Evolutionary Computation Conference Companion, pp. 915–918. Association for Computing Machinery, ??? (2025). https://doi.org/10.1145/3712255.3726740 . https://doi.org/10.1145/3712255.3726740

[21] Kumar, S., Lai, T.H., Arora, A.: Barrier coverage with wireless sensors. In: Proc. ACM MobiCom, pp. 284–298 (2005). https://doi.org/10.1145/1080829.1080859

[22] Ban, D., Jiang, J., Yang, W., Wen, J., Dou., W.: Energy-efficient algorithms for k-barrier coverage in mobile sensor networks. Int. J. Comput. Commun. Control **5**(5), 616–624 (2010)

[23] Chen, G., Xiong, Y., She, J.: A k-barrier coverage enhancing scheme based on gaps repairing in visual sensor network. IEEE Sensors Journal **23**(3), 2865–2877 (2023) https://doi.org/10.1109/JSEN.2022.3227601

[24] He, S., Chen, J., Li, X., Shen, X., Sun, Y.: Leveraging prediction to improve the coverage of wireless sensor networks. IEEE Trans. Parallel Distrib. Syst. **23**(4), 701–712 (2012) https://doi.org/10.1109/TPDS.2011.180

[25] Wang, Y., Cao, G.: Barrier coverage in camera sensor networks, pp. 12–11210 (2011). https://doi.org/10.1145/2107502.2107518

[26] Liu, B., Dousse, O., Wang, J., Saipulla, A.: Strong barrier coverage of wireless sensor networks, pp. 411–420. Association for Computing Machinery, ??? (2008). https://doi.org/10.1145/1374618.1374673

[27] Cheng, W.-F., Liu, K., Liu, Y., Li, X.-Y., Liao, X.-K.: Sweep coverage with mobile sensors. IEEE Trans. Mobile Comput. **10**(8), 1534–1545 (2011) https://doi.org/10.1109/IPDPS.2008.4536245

[28] Luong, H.V.D., Binh, H.T.T., Binh, N.T.M., Chien, T.V.: Mobile device-target association optimization for connectivity enhancement in wireless IoT sensor networks. Cluster Computing **28**(15), 978 (2025) https://doi.org/10.1007/s10586-025-05647-9

[29] Binh, N.T.M., Luong, H.V.D.: Solving of the maximal exposure path problem in heterogeneous directional wireless sensor networks using an improved genetic algorithm. Journal of Computer Science and Cybernetics **41**(2), 163–180 (2025) https://doi.org/10.15625/1813-9663/21945

[30] Karatas, M.: Optimal deployment of heterogeneous sensor networks for a hybrid point and barrier coverage application. Computer Networks **132** (2018) https://doi.org/10.1016/j.comnet.2018.01.001

[31] My, B.N.T., Thi, A.L.: A weighted-sum approach for multi-objective optimization

of strong barrier coverage in IoT heterogeneous wireless sensor networks. In: Proc. ICCIES, pp. 267–280 (2025). https://doi.org/10.1007/978-3-031-98167-8_20

[32] Funke, D., Hespe, D., Sanders, P., Storandt, S., Truschel, C.: Pareto sums of pareto sets: Lower bounds and algorithms. Algorithmica **87**(8), 1111–1144 (2025) https://doi.org/10.1007/s00453-025-01314-y

[33] Gunantara, N.: A review of multi-objective optimization: Methods and its applications. Cogent Engineering **5** (2018) https://doi.org/10.1080/23311916.2018.1502242

[34] Chaudhari, P., Thakur, A., Kumar, R., Banerjee, N., Kumar, A.: Comparison of nsga-iii with nsga-ii for multi objective optimization of adiabatic styrene reactor. Materials Today: Proceedings **57** (2021) https://doi.org/10.1016/j.matpr.2021.12.047

[35] Tran, H.-A., Duong, C.-S., Bui, T.-D., Tong, V., Binh, H.T.T.: Gamr: Revolutionizing multi-objective routing in sdn networks with dynamic genetic algorithms. IEEE Transactions on Emerging Topics in Computational Intelligence **9**(4), 3147–3161 (2025) https://doi.org/10.1109/TETCI.2025.3543836

[36] Liang, J., Ban, X., Yu, K., Qu, B., Qiao, K., Yue, C., Chen, K., Tan, K.C.: A survey on evolutionary constrained multiobjective optimization. IEEE Transactions on Evolutionary Computation **27**(2), 201–221 (2023) https://doi.org/10.1109/TEVC.2022.3155533

[37] Ma, L., Dai, C., Xue, X., Peng, C.: A multi-objective particle swarm optimization algorithm based on decomposition and multi-selection strategy. Computers, Materials & Continua **82**, 997–1026 (2025) https://doi.org/10.32604/cmc.2024.057168

[38] Konstantinidis, A., Yang, K.: Multi-objective K-connected deployment and power assignment in WSNs using a problem-specific constrained evolutionary algorithm based on decomposition. Computer Communications **34**(1), 83–98 (2011) https://doi.org/10.1016/j.comcom.2010.08.011

[39] Binh, N.T.M., Nghia, N.T., Huy, N.Q., Luong, H.V.D.: Obstacle-aware multiobjective evolutionary optimization for maximal exposure path planning in iot-enabled heterogeneous sensor networks. In: Proceedings of the Genetic and Evolutionary Computation Conference Companion (2026). https://doi.org/10.1145/3795101.3805366 . https://doi.org/10.1145/3795101.3805366

[40] Sree, K.R., Pamula, V.K.: Performance-aware deployment of heterogeneous sensors in wireless sensor networks via multi-objective nspso. Microsystem Technologies **32**(2), 12 (2026)